UNIVERSIDADE FEDERAL DE SANTA MARIA
CENTRO DE TECNOLOGIA
PROGRAMA DE PÓS-GRADUAÇÃO EM ENGENHARIA QUÍMICA

Enrique Chaves Peres

PRODUÇÃO E CARACTERIZAÇÃO DE NANO SÍLICA MODIFICADA OBTIDA DE CASCA DE ARROZ PARA A UTILIZAÇÃO COMO ADSORVENTE DE CORANTES

Santa Maria, RS, Brasil

2018

Enrique Chaves Peres

PRODUÇÃO E CARACTERIZAÇÃO DE NANO SÍLICA MODIFICADA OBTIDA DE CASCA DE ARROZ PARA A UTILIZAÇÃO COMO ADSORVENTE DE CORANTES

Dissertação apresentada ao Curso de Mestrado do Programa de Pós-Graduação em Engenharia Química, Área de Concentração em Desenvolvimento de Processos Industriais e Ambientais, da Universidade Federal de Santa Maria (UFSM, RS), como requisito parcial para obtenção do grau de **Mestre em Engenharia Química.**

Orientador: Prof. Dr. Guilherme Luiz Dotto

Santa Maria, RS

2018

Ficha catalográfica elaborada através do Programa de Geração Automática
da Biblioteca Central da UFSM, com os dados fornecidos pelo(a) autor(a).

Peres, Enrique
PRODUÇÃO E CARACTERIZAÇÃO DE NANO SÍLICA MODIFICADA OBTIDA DE CASCA DE ARROZ PARA A UTILIZAÇÃO COMO ADSORVENTE DE CORANTES / Enrique Peres.- 2018.
95 p.; 30 cm

Orientador: Guilherme Luiz Dotto
Coorientador: Edson Luiz Foletto
Dissertação (mestrado) - Universidade Federal de Santa Maria, Centro de Tecnologia, Programa de Pós-Graduação em Engenharia Química, RS, 2018

1. Adsorção 2. Sílica 3. Nano-partículas 4. Lixiviação I. Dotto, Guilherme Luiz II. Foletto, Edson Luiz III. Título.

Enrique Chaves Peres

PRODUÇÃO E CARACTERIZAÇÃO DE NANO SÍLICA MODIFICADA OBTIDA DE CASCA DE ARROZ PARA A UTILIZAÇÃO COMO ADSORVENTE DE CORANTES

Dissertação apresentada ao Curso de Mestrado do Programa de Pós-Graduação em Engenharia Química, Área de Concentração em Desenvolvimento de Processos Industriais e Ambientais, da Universidade Federal de Santa Maria (UFSM, RS), como requisito parcial para obtenção do grau de **Mestre em Engenharia Química.**

Aprovado em 15 de janeiro de 2018:

_____
Guilherme Luiz Dotto, Dr. (UFSM)
(Presidente/Orientador)

_____
Evandro Stoffels Mallmann, Dr. (UFSM)

_____
Tito Roberto Sant'Anna Cadaval Junior, Dr. (FURG)

Santa Maria, RS
2018

AGRADECIMENTOS

Venho através destes, agradecer a todos que fizeram parte deste trabalho, e me ajudaram nesta longa jornada para a obtenção do título de mestre, em especial ao citados abaixo:

À Deus, e a todos que espiritualmente me guiaram nesse caminho;

À minha mãe, Cilda, por ser minha companheira durante este percurso, sendo a base da minha vida, proporcionando-me todas condições para poder completar o mestrado;

Ao meu pai Luiz e meu irmão Eder, pelo apoio, carinho e compreensão ao longo destes anos e a ajuda nos momentos mais cruciais desta jornada;

Ao meu orientador, Prof. Dr. Guilherme Luiz Dotto, principalmente pelo acolhimento em uma cidade diferente, sendo quase um segundo pai neste caminho, além da oportunidade a mim dada de desenvolver este projeto, pelos ensinamentos e confiança depositada;

Aos Prof. Dr. Evandro Mallmann e Dr. Edson Foletto pela ajuda neste estudo e pelas oportunidades oferecidas ao passar destes dois anos;

Aos alunos de iniciação cientifica, que me acompanharam neste percurso, ajudando nos experimentos, em especial a Jenifer Slaviero, que esteve desde o começo deste trabalho, e sem ela este trabalho não seria possível;

Ao Programa de Pós-Graduação em Engenharia Química da Universidade Federal de Santa Maria, incluindo professores e funcionários, pela estrutura, ambiente e serviços prestados direta e indiretamente durante a elaboração desta pesquisa;

Aos colegas do Programa de Pós-graduação em Engenharia Química pelo companheirismo, momentos de descontração e auxílios prestados ao longo destes dois anos.

RESUMO

PRODUÇÃO E CARACTERIZAÇÃO DE NANO SÍLICA MODIFICADA OBTIDA DE CASCA DE ARROZ PARA A UTILIZAÇÃO COMO ADSORVENTE DE CORANTES

AUTOR: Enrique Chaves Peres

ORIENTADOR: Prof. Guilherme Luiz Dotto

O aumento da produção de resíduos agroindustriais ao redor do mundo consolida a busca por alternativas para utilização destes materiais de forma a agregar valor. Entre os materiais com maior produção em escala mundial, destaca-se a casca de arroz, utilizada em grande escala no setor industrial para a geração de energia. A queima da casca gera novamente resíduos sólidos, sendo este um dos principais problemas enfrentados, o tratamento do resíduo inorgânico produzido. Muitos trabalhos publicados nos últimos anos utilizaram-se das rotas de purificação para produção da sílica obtida da casca do arroz, porém na maior parte dos trabalhos não há utilização posterior e poucas rotas para melhoria do material produzido. Neste sentido, a mudança na rota de lixiviação para a purificação e a posterior produção de nanopartículas mostra-se como meio de valorização do resíduo da casca de arroz. Este trabalho se propõe a investigar a utilização de ultrassom e micro-ondas na etapa de lixiviação para a produção de nanopartículas de sílica ($nSiO_2$) a partir da casca do arroz, e posterior utilização na adsorção de corantes da indústria têxtil. Para isso, foram produzidos três tipos diferentes de nanopartículas de sílica, como segue: utilizando métodos convencionais para lixiviação ($nSiO_2$), utilizando ultrassom (UM-$nSiO_2$) e utilizando micro-ondas (MW-$nSiO_2$). Em um primeiro momento, foram caracterizadas as nanopartículas produzidas para obtenção de dados referentes aos grupos funcionais presentes (FT-IR), tamanho de poros (BET), cristalinidade (DRX), propriedades térmicas (DSC), tamanho de partículas (MEV) e massa especifica. Após, foram realizados testes para adsorção de violeta cristal utilizando a amostra padrão e modificada com ultrassom, sendo analisados como parâmetros a dosagem de adsorvente (variando de 0,1 a 1 g L^{-1}), o pH (variando de 2 a 10), o tempo de adsorção (variando de 0 a 240 min) e a temperatura (variando de 25 a 55°C). Através dos dados obtidos, foram realizados os ajustes a modelos cinéticos e de isotermas para ambos os adsorventes. A amostra modificada com ultrassom apresentou capacidade de adsorção superior (495 mg g^{-1}) e maior remoção do corante (98%) comparada a amostra padrão(424 mg g^{-1}) para a remoção de Cristal Violeta.Para o segundo estudo, a amostra padrão ($nSIO_2$) e amostra modificada com micro-ondas (MW-$nSiO_2$) foram utilizadas para adsorção de azul de metileno. Foram realizadas as mesmas variações do primeiro estudo, obtendo-se uma capacidade de adsorção maior para a MW-$nSiO_2$ (679 mg g^{-1}) comparada a nSiO2 (547 mg g^{-1}) para o corante azul de metileno. Ambas as modificações das nanopartículas, mostram-se promissoras devido ao aumento da área superficial das partículas produzidas, acarretando em melhores características para adsorção.

Palavras-chave: Adsorção, casca de arroz, lixiviação, nano partículas, Sílica

ABSTRACT

PRODUCTION AND CHARACTERIZATION OF MODIFIED NANO SILICA FROM RICE HUSK FOR DYE REMOVAL

AUTHOR: Enrique Chaves Peres

ADVISOR: Dr. Guilherme Luiz Dotto

The large generation of agro-industrial wastes around the world requires the search for alternatives to use these materials. Among the materials, rice husks are used in large scale in the industrial sector for energy generation. The husk burning generates solid residues, being this one of the main problems faced, the treatment of the inorganic residue produced. Many papers published in recent years have used purification routes to produce silica obtained from rice husks, but in most of the works, there is no later use and few routes to improve the material produced. In this sense, the change in the leaching route for the purification and subsequent production of nanoparticles is shown as a means of valorizing the rice husk residue. This work proposes to investigate the use of sonication and microwaves in the leaching process for the production of silica ($nSiO_2$) nanoparticles from the rice husk and subsequent use in the adsorption of terxtile dyes. For this, three different types of silica nanoparticles were produced: using conventional methods for leaching ($nSiO_2$), using ultrasound (UM-$nSiO_2$) and using microwaves (MW-$nSiO_2$). At first, the nanoparticles were characterized according to the functional groups (FT-IR), pore size (BET), crystallinity (XRD), calorimetric properties (DSC), particle size (SEM) and specific mass. After that, tests were carried out for the adsorption of crystal violet using the standard and ultrasonic-modified samples. The following parameters were analyzed: adsorbent dosage (ranging from 0.1 to 1 g L^{-1}), pH (ranging from 2 to 10), the adsorption time (ranging from 0 to 240 min) and the temperature (ranging from 25 to 55 °C). By means of the obtained data, the adjustments were made to kinetic and isothermal models for both adsorbents. The ultrasound-modified sample (UM-$nSiO_2$) showed superior adsorption capacity (495 mg g^{-1}) and greater dye removal (98%) compared to the standard sample (424 mg g^{-1}) ($nSiO_2$) to remove Crystal violet. For the second article, the standard sample ($nSIO_2$) and sample modified with microwaves (MW-$nSiO_2$) were used for adsorption of methylene blue. The same variations of the first article were performed, obtaining a greater adsorption capacity for MW-$nSiO_2$ (679 mg g^{-1}) compared to $nSiO_2$ (547 mg g^{-1}) for the methylene blue dye. Both modifications of the nanoparticles show promise due to the increased surface area of the particles produced, leading to better adsorption characteristics.

Keywords: Adsorption, rice husk, leaching, nanoparticles, silica

ÍNDICE DE FIGURAS

ÍNDICE DE TABELAS

SUMÁRIO

1. INTRODUÇÃO

A busca por alternativas para o uso de resíduos sólidos gerados através da agroindústria é um grande desafio para empresas e produtores em âmbito mundial. A grande produção desses materiais, que possuem um baixo valor agregado, evidencia a necessidade do tratamento para valorização dos mesmos. Dentre estes resíduos destacam-se a produção de casca de arroz, quirera de arroz, palha de milho entre outros que poderiam ser reaproveitados (IRGA, 2017). Segundo dados do Instituto Rio-Grandense de Arroz (IRGA), no Rio Grande do Sul, maior produtor do grão, a produção de arroz no ano de 2017 foi cerca de 8,3 $x10^6$ toneladas, gerando assim toneladas de outra biomassa, a casca de arroz (BELCHIOR; TAI; HELD, 2017). O principal destino da casca de arroz é a queima para geração de energia, tendo como resíduos as cinzas. Atualmente, empresas do estado buscam alternativas para a venda deste resíduo, porém, as impurezas do material gerado e o alto valor para purificá-lo acarretam problemas na comercialização. O tipo de casca de arroz e suas propriedades dependem da localização, cor e as variações climáticas que ocorrem no período de crescimento da planta (TSAI; LEE; CHANG, 2007).

A composição das cinzas é basicamente de óxidos, principalmente dióxido de silício que pode atingir uma pureza maior que 99% (XIONG et al., 2009), se for realizado um tratamento adequado. O dióxido de silício (SiO_2) é um composto semicondutor, que devido as suas características físico-químicas pode ser utilizado em diversos setores. Pode-se citar como exemplo: o uso como aditivo no concreto, aumentando a resistência e diminuindo a permeabilidade, a fabricação de células fotovoltaicas, para geração de energia, e a fabricação de componentes eletrônicos, como a produção de microchips e transistores (AGGARWAL; SINGH; AGGARWAL, 2015; KAMAT, 2008; XIA et al., 2005). Além disso, pode ser utilizada como aditivo de polímeros, ou pode ser utilizada como reagente na formação de carbeto de silício (SiC), esse utilizado para a fabricação de componentes eletrônicos (SINGH et al., 2008). Há pesquisas relacionadas a utilização de sílica como adsorvente, para a remoção de compostos metálicos, porém não são encontrados estudos do uso de nano sílica e modificações na mesma para a utilização de compostos orgânicos (FOLETTO et al., 2005).

A produção de sílica a partir da casca do arroz possui diversas rotas, porém podemos citar quatro processos que inicialmente são utilizados: tratamento térmico, hidrotérmico, biológico ou químico (SOLTANI et al., 2015). Dentre estes processos o mais utilizado é o tratamento térmico. Este se baseia na queima da matéria prima a temperaturas elevadas (400 °C a 700 °C) para inicialmente produzir sílica amorfa e após é feita lixiviação com ácidos para a purificação da sílica. Após este processo é realizado um aquecimento a temperatura de 700 °C a 1200 °C para a produção de nano partículas de sílica, sendo que essa sofrerá alterações nas suas propriedades superficiais através de métodos de degradação. A maioria dos processos de produção de nano sílica ocorre apenas com a etapa de elevação de temperatura, (1000 °C – 1200 °C), como exemplo deste temos a produção através da casca de arroz. Porém, há outros tipos de processos, como a dissolução hidrotérmica de vidro para obtenção posterior de nanoSiO_2 e a utilização de decomposição da olivina ($(Mg,Fe)_2SiO_4$) como reagente. (LAZARO et al., 2013).

Atualmente, há diversas utilizações de nanopartículas, que abrangem desde áreas como polímeros até o setor de cosméticos (GUPTA et al., 2013). No uso de nanomateriais como adsorventes, tem se como principal vantagem a melhoria das propriedades de superfície do material, aumentando a razão entre a superfície e o volume. Através desta melhoria, a nano sílica produzida pode ter um melhor desempenho que outros adsorventes. Normalmente, os materiais adsorventes mais utilizados são: carvão ativado, sílica gel e zeólitas. Estes materiais destacam-se devido a apresentarem características de alta porosidade, seletividade e baixo custo, mas principalmente pela grande área superficial desses (GUPTA; SUHAS, 2009) .

Segundo dados da Associação Brasileira de Fabricantes de Tintas (ABRAFATI), o Brasil é um dos seis maiores países fabricante de compostos que possuem corantes do mundo, produzindo cerca de 1,506 bilhões de litros por ano, gerando assim uma grande quantidade de resíduos que devem ser tratados para serem descartados no meio ambiente. Devido a isso, a utilização de um resíduo sólido de baixo custo para a remoção de substâncias contaminantes ao meio ambiente, como corantes presentes nas tintas, diminuiria os custos para a indústria, além de ser uma solução prática tanto para a agroindústria quanto para os setores que geram efluentes coloridos.

2 OBJETIVOS

2.1. OBJETIVO GERAL

O objetivo desta dissertação é produzir e caracterizar a nanoSiO_2 obtida da casca de arroz, modificando-a através de métodos como o uso de micro-ondas e ultrassom para utilização como adsorvente de corantes.

2.2. OBJETIVOS ESPECÍFICOS

- Preparar nanoSiO_2 a partir de casca de arroz através de um processo convencional;
- Preparar nanoSiO_2 a partir da casca de arroz utilizando um processo modificado por ultrassom;
- Preparar nanoSiO_2 a partir da casca de arroz utilizando um processo modificado por micro-ondas;
- Caracterizar as diferentes nanoSiO_2 obtidas utilizando análise de infravermelho (FT–IR), difração de raios X (DRX), isotermas de N_2 (métodos BET e BJH), picnometria de gás hélio, fluorescência de raios X (XRF), calorimetria exploratória diferencial (DSC) e microscopia eletrônica de varredura (MEV)
- Avaliar os efeitos do ultrassom e do micro-ondas nas características das nanoSiO_2 obtidas, em relação ao processo convencional;
- Estudar o potencial adsorvente das diferentes nanoSiO_2 para remover os corantes azul de metileno e cristal violeta de soluções aquousas;
- Estudar o perfil cinético, comportamento de equilíbrio e parâmetros termodinâmicos da adsorção dos corantes pelas diferentes nanoSiO_2.

3 REVISÃO BIBLIOGRÁFICA

3.1 GERAÇÃO DE CASCAS DE ARROZ

Segundo dados do Departamento de Agricultura dos Estados Unidos (USDA) a produção mundial de arroz em 2016 foi de 483,1 milhões de toneladas, sendo o segundo cereal mais colhido, atrás apenas da produção de trigo. A produção de arroz está localizada principalmente no continente asiático, sendo 90 % da produção total do grão. Como maior produtor de arroz destaca-se a China com cerca de 30 % da produção mundial. O Brasil é o nono colocado entre os países produtores, com 1,6 % em relação a produção mundial. Na produção nacional, 71,4% do arroz produzido é originado no estado do Rio Grande do Sul (BELCHIOR; TAI; HELD, 2017). Na Figura 1 tem-se a evolução do preço da casca de arroz (principal resíduo gerado) no estado do Rio Grande do Sul, mostrando uma grande desvalorização em relação ao tempo.

Figura 1 – Preço médio da casca de arroz no período de janeiro de 1975 a setembro de 2017

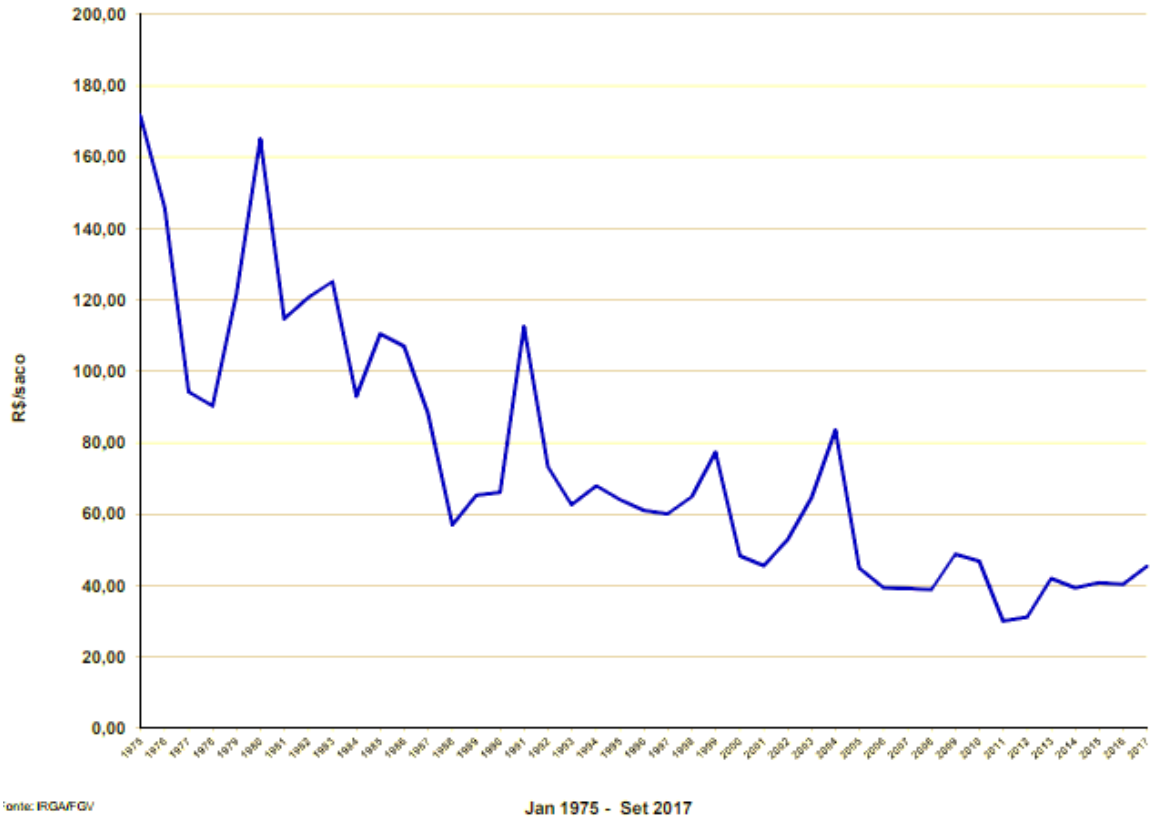

Fonte: Adaptado do Relatório Anual de Produção de Arroz, IRGA, 2017.

A casca de arroz é um dos principais resíduos originados da produção de arroz. Há outros resíduos da produção do arroz que podem ser citados como: a quirera, a palha de arroz e o farelo de arroz. Porém, o volume de produção da casca de arroz é maior em relação aos demais resíduos, sendo cerca de 20% da massa total do grão. (MAYER; HOFFMANN; RUPPENTHAL, 2006).

O principal uso da casca de arroz é para a geração de energia. Essa é queimada como resíduo em caldeiras, isto ocorre devido à grande quantidade de casca, o baixo custo e a falta de alternativas para a geração de um produto de maior valor agregado (YOON et al., 2012). O uso para a geração de energia acaba gerando outro resíduo: as cinzas. Atualmente, as cinzas possuem valor ainda menor que a casca de arroz, sendo que para a sua utilização necessitam de um processo de purificação.

3.2 COMPOSIÇÃO DA CASCA DE ARROZ

A casca de arroz é composta principalmente por compostos orgânicos: lignina, celulose, hemicelulose. Além destes, pode se citar a presença de compostos inorgânicos, como o dióxido de silício (SiO_2) como sendo o constituinte inorgânico de maior quantidade presente na biomassa. A composição da casca de arroz está demonstrada na Figura 2, estes dados foram retirados segundo Hickert et. al, 2010 de uma arrozeira presente na cidade de Pelotas.

Figura 2 - Composição da casca de arroz na região sul do Brasil

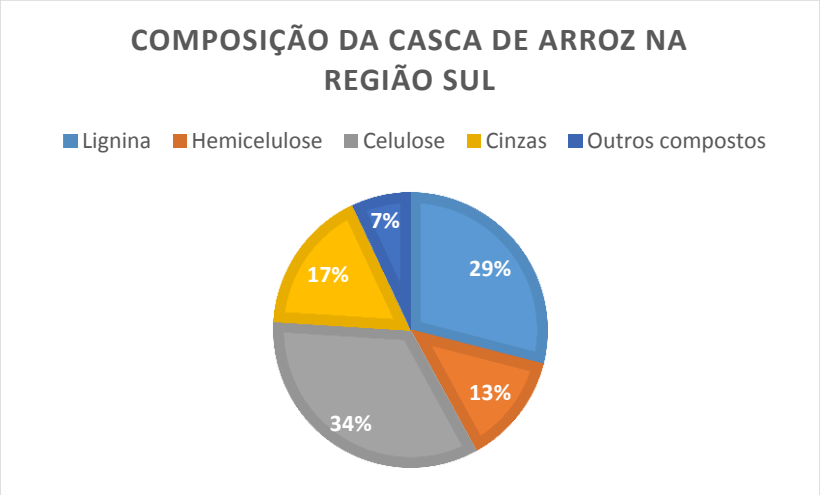

Fonte: Adaptado de Hickert (2010)

Em temperaturas altas, a matéria orgânica presente na casca reage formando gases como dióxido e monóxido de carbono, sendo assim os produtos resultantes são apenas os compostos inorgânicos presentes na amostra (JI-LU, 2007). Há variações na composição da casca, principalmente devido a mudanças climáticas que interferem na safra ou localização geográfica das plantações.

3.3 COMPOSIÇÃO INORGÂNICA DA CASCA DE ARROZ E PRINCIPAIS UTILIZAÇÕES

Entre os compostos inorgânicos presentes na casca de arroz, o dióxido de silício é o que possui maior fração mássica, como demonstrado na Tabela 1. Segundo Patel et. al. 1987, há também a presença de outros óxidos como de Ferro II, cálcio e alumínio.

Tabela 1 - Composição Inorgânica da casca de arroz

Composto	% mássica
Al_2O_3	4,935
Fe_2O_3	5,136
CaO	4,975
MgO	0,8426
SiO_2	88,75
MnO_2	0,2969

Fonte: Adaptado de Patel, 1987

O dióxido de silício, também conhecido como sílica, é um composto semicondutor muito utilizado para produção em materiais eletrônicos. Porém, devido as suas características físico químicas, pode ser utilizado como aditivo no cimento ou borracha, modificando características como rigidez e resistência mecânica. Além disso, a sílica pode ser usada como adsorvente, suporte para catálise ou síntese de zeólitas. A sílica pode ser classificada como aquagel (poros são preenchidos com água), xerogel (fase aquosa dos poros é removida por evaporação) e aerogel (solvente é removido por extração supercrítica) (FOLETTO et al., 2005).

A sílica pode ser produzida da casca de arroz com uma pureza de até 99,66%, sendo obtida através do tratamento ácido das cinzas obtidas da casca de arroz (YALÇIN; SEVINÇ, 2001). Os principais ácidos utilizados para o processo de lixiviação são o ácido clorídrico, sulfúrico ou nítrico, variando a concentração desses como parâmetro. De acordo com Soltani, 2015, é possível obter uma pureza maior com o ácido clorídrico em concentrações acima de 3 M. No tratamento com ácido sulfúrico, resulta em maior contaminação, devido a concentração de cálcio, que é maior quando comparada aos demais ácidos.

Há outros fatores importantes para a obtenção de sílica de alta pureza, como o tempo de lixiviação, o tempo de queima da matéria orgânica e a temperatura de queima afetam diretamente a pureza da sílica e a estrutura da sílica (cristalina ou amorfa).

3.4 NANO SÍLICA

A nano tecnologia é uma área de grande potencial que têm se expandido devido a vasta área de utilização das nano partículas. Estas podem ser aplicadas para modificação de materiais existentes ou para inovação tecnológica, como o uso em adsorção de gases. De acordo com Wang, L, 2015, nano sílica porosa pode ser utilizada para adsorção de metano em presença de água.

Segundo Yao, et al, 2013, a nano sílica é um nano composto que possui como características principais uma grande área de superfície para adsorção, boa dispersão, pureza química elevada e excelente estabilidade. Além disso, pode se citar o baixo custo e possui uma alta taxa de produção como vantagens da nano sílica em relação a outros nano materiais.

3.4.1 Principais aplicações

A nano sílica pode ser utilizada como aditivo de concretos. Segundo Biricik e Sarier, 2014, a presença de nano sílica permite uma maior densidade na zona de transição do concreto, além de possuir maior resistência que o concreto comum (BIRICIK; SARIER, 2014). Outro uso comum de nano sílica é a utilização como

aditivo em polímeros, como o polipropileno para diminuição da inflamabilidade do material, de acordo com Erdem, et.al 2009.

Além destes usos, a nano sílica pode ser utilizada ainda na indústria de cosméticos e como aditivo na produção de embalagens de produtos comestíveis. Porém, estes usos tem diminuído devido a estudos sobre os riscos à saúde, essa poderia causar ao corpo humano danos ao sistema digestivo.(PETERS et al., 2009).

3.4.2 Métodos de produção

Nano sílica são partículas de sílica em escala nanométrica sendo que a alteração no processo de produção é realizada após a lixiviação. Existem vários processos para a produção de sílica a partir da casca de arroz, destacando-se: o tratamento térmico, o tratamento hidrotérmico, o tratamento biológico e o tratamento químico (SOLTANI et al., 2015). Dentre esses, os mais utilizados são o tratamento térmico e o tratamento químico.

O tratamento térmico ocorre primeiramente a partir da queima da casca de arroz a temperaturas de 400 a 700 °C para a produção das cinzas. Após pode ser realizado três rotas diferentes: tratamento alcalino com hidróxido de sódio, adição de NH_4F ou lixiviação ácida. O pré-tratamento da sílica com ácido é o mais utilizado entre estes métodos, sendo feita uma lixiviação para remoção das impurezas presente na sílica, através da reação 1.

$$SiO_2 + R.O + HCl \rightarrow R.Cl + SiO_2 + H^+ + O^- \quad (1)$$

O tratamento químico ocorre através da reação com compostos alcalinos, lixiviação ácida ou tratamento com compostos como peróxido de hidrogênio. Este tratamento é similar ao tratamento térmico, apenas invertendo a ordem do processo, sendo que no tratamento químico tem-se a reação para a retirada de compostos e após a queima da matéria orgânica presente, sendo que o inverso ocorre no tratamento térmico.

De acordo com Chandrasekhar et.al ,2006, no tratamento térmico, a temperatura de queima afeta diretamente a estrutura da sílica. A temperaturas maiores que 900°C a sílica apresenta estrutura cristalina e a temperaturas abaixo de 800°C esta é amorfa. Além disso, segundo Dafalla, 2010, apenas a temperaturas acima de 600°C é possível remover todos os compostos orgânicos presentes na casca de arroz

(CHANDRASEKHAR et al., 2003). Outro fator importante é o tempo de queima, maiores concentrações de dióxido de silício são encontradas com tempos superiores a 6 horas.

Há dois métodos mais utilizados para a produção de nano partículas: através da dissolução hidrotérmica de silicato de sódio ou através da hidrólise e queima de tetracloreto de silício (LAZARO et al., 2012). De acordo com Sankar et al, 2015, a nano sílica pode ser produzida a partir da sílica da casca de arroz através de um processo de aquecimento para a diminuição do tamanho de partícula. Este processo deve ocorrer com uma taxa de aquecimento de 5°C/min em um período de 2 horas. Segundo Liou, 2004, esta taxa deve ser utilizada para aumento do tamanho dos poros da nano sílica.

3.5 MODIFICAÇÃO COM ULTRASSOM

O uso do ultrassom para a utilização em adsorção foi estudado por Breitarch, Bathen e Schmift-Traubt, 2003, devido à grande quantidade de informações controversas sobre o tema. A cavitação gerada pelo ultrassom pode acarretar um aumento da transferência de calor e massa, além de erosão nas partículas, isto acarretaria um aumento da área superficial beneficiando a adsorção, ou no caso deste trabalho a lixiviação do material. Na Figura 3, é possível visualizar o aumento do número de poros devido a utilização da sonda ultrassônica.

Figura 3 - Modificação de nano partículas de SiO_2 através de ultrassom

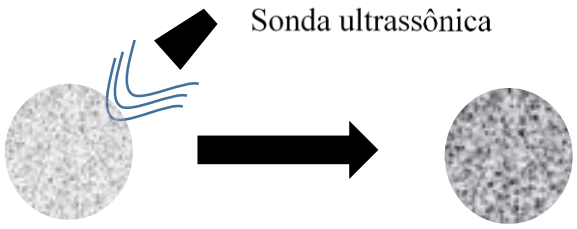

Fonte: Autor

Geralmente a utilização do ultrassom aumenta a taxa de reação, em casos como a lixiviação isto pode acarretar em menores tempos de residência para o mesmo rendimento de um processo padrão. De acordo com Singh et. al, 1998, diversos

compostos podem ser sintetizados como álcoois e alquenos, aumentando o rendimento final em relação ao convencional.

3.6 MODIFICAÇÃO COM MICRO-ONDAS

O uso de radiação via micro-ondas para alteração de propriedades químico-físicas ou alteração de processos já existentes têm aumentado nos últimos anos. Micro-ondas são ondas que possuem um comprimento de onda na faixa entre 0,3 m até 1 mm) (HALLIDAY; RESNICK; WALKER, 2009).

De acordo com Larhed e Olofsson, 2006, o micro-ondas é utilizado para aumentar a taxa de reação, principalmente em sínteses orgânicas, um exemplo deste é a síntese de alcaloides como o TMC 120B ($C_{15}H_{13}NO_2$), sendo esta substância utilizada para a fabricação de remédios.

Segundo Kappe e Dallinger, 2004, o uso de micro-ondas depende principalmente das propriedades dielétricas do composto, principalmente do solvente utilizado, sendo que a característica que permite converter energia eletromagnética em calor, sendo função da temperatura e frequência, é chamada de fator de perda (tan δ).

De acordo com Lidstrom et al, 2001, a grande vantagem do uso de micro-ondas é que essas atravessam as paredes do recipiente agindo diretamente na solução e acarretando um aumento da temperatura uniforme. Portanto, há homogeneidade da solução final, devido ao modelo transferência de calor utilizada em relação a métodos tradicionais de aquecimento, como chapas de aquecimento como demonstrado na Figura 4.

Figura 4 - Diferença entre os métodos de transferência de calor através de ondas

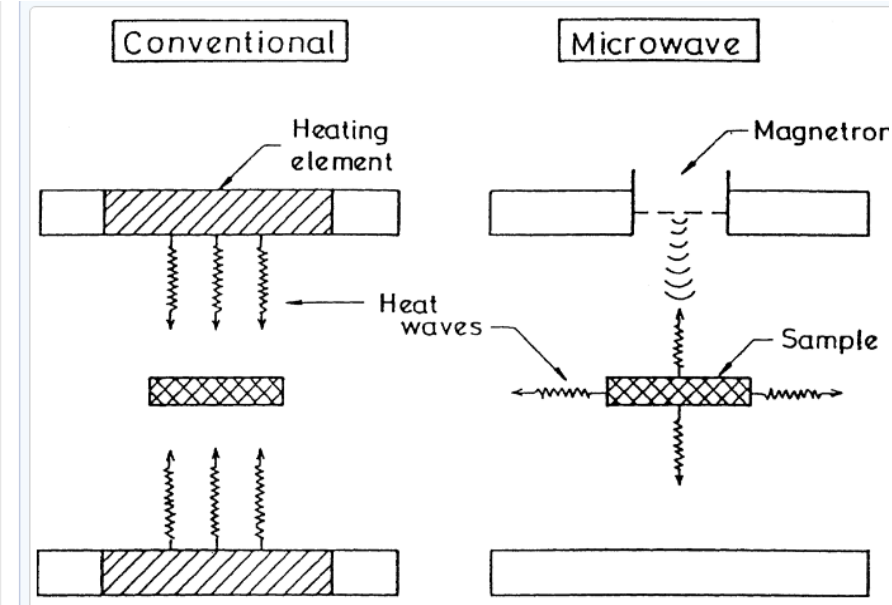

Fonte – Adaptado de Rao,et al. 1999

3.7 EFLUENTES/RESÍDUOS GERADOS NO SETOR DE CORANTES

De acordo com Chiou, Ho e Li, 2004, a remoção da cor em efluentes industriais tornou-se um dos principais problemas ambientais no setor industrial no setor de tintas, isto ocorre, por que uma pequena quantidade de corante na água pode ser tóxica e visível (CHIOU; HO; LI, 2004). Conforme Malik, Rawteke e Wate, 2007, aproximadamente 1 miligrama por litro de corante já pode ser visível podendo causar intoxicação, portanto imprópria para consumo (MALIK; RAMTEKE; WATE, 2007).

Segundo dados Leão et al 2002, em uma indústria é utilizado aproximadamente 128 litros de água para cada quilograma de tecido que é produzido. Além disso estima-se que 88% do volume de água é descartado e os outros 12% correspondem as perdas evaporativas do processo (LEÃO, 2002).

3.8 LEGISLAÇÃO AMBIENTAL

Os corantes utilizados foram Cristal Violeta (CV) e Azul de Metileno (MB), ambos catiônicos, sendo estes utilizados principalmente para a coloração de fibras têxteis. Dentro das características físico-químicas destacam-se as altas massas

moleculares de 394 e 320 gramas por mol, para o Cristal Violeta e o Azul de Metileno, respectivamente. Em relação a informações toxicológicas, a exposição por um longo período a estes corantes pode ter efeito cancerígeno ao sistema imunológico (SALLEH et al., 2011).

Segundo Almeida 2006, os corantes podem ser classificados primeiramente como orgânicos ou inorgânicos e após em dois outros subgrupos que são sintéticos ou naturais. Além disso, classifica-se o corante segundo sua estrutura química ou método em que é fixado na fibra têxtil (ALMEIDA, 2006). Deste modo há oito classificações de corantes: reativos, diretos, azoicos, ácidos, sulfurosos, dispersos, pré-metalizados e básicos.

Em relação aos grupos, pode-se destacar o grupo de corantes básicos. Esta classe de corantes possui íons carregados positivamente, atraindo assim compostos negativos. Além disso, destaca-se que este grupo de corantes possui grande solubilidade em água, dificultando o tratamento do efluente quando presente nos resíduos de indústrias têxteis (GUARATINI; ZANONI, 1999).

3.9 PRINCIPAIS MÉTODOS DE TRATAMENTO

O efluente líquido gerado na indústria têxtil pode ser tratados através de métodos químico, físicos e biológicos. De acordo com Wang et.al 2011, como métodos físico-químicos destacam-se a flotação, coagulação/floculação/sedimentação, processos oxidativos avançados, adsorção e processos de filtração com membranas. Nos processos biológicos podem-se utilizar meios tanto aeróbicos como anaeróbicos para o tratamento destes efluentes .

. O principal método para o tratamento de águas contaminadas com corantes é a adsorção, devido a ser um método barato e o adsorvente pode ser recuperado. De acordo com Weber e Chakravorti et al, 1974 pode-se citar a menor área superficial, a facilidade de operação e a maior remoção dos contaminantes orgânicos

3.10 ADSORÇÃO

De acordo com Yagub et al, 2014, adsorção é o fenômeno que descreve o partição de uma substância entre duas fases (líquido-sólido e gás-sólido). A substância que acumula na interface é chamada de adsorbato, enquanto o sólido é chamado de adsorvente.

Segundo Dabrowski, 2001, os adsorventes porosos mais utilizados são carbonos ativados e zeólitas, porém atualmente, há diversas pesquisas relacionadas a diminuição do tamanho de poros, principalmente na área de materiais nanoporosos. Os usos destes materiais têm aumentado em consequência das diversas aplicações como separação, purificação e processos catalíticos.

Há diversos fatores que influenciam na adsorção de corantes, como a concentração do mesmo, a dosagem de adsorbato, o pH da solução, a temperatura e o tempo do processo. Segundo Seow e Lim, 2016, estes fatores são fundamentais para a mudança para escala industrial.

3.10.1 Efeito da dosagem de adsorvente

A quantidade de adsorvente é um dos fatores que afeta diretamente os processos de adsorção, pois o adsorvente representa um alto custo dependendo do corante que será removido. A busca por um material adsorvente de baixo custo, com baixa dosagem para adsorção e que possa ser recuperado com processos simples é um dos maiores desafios do setor de adsorção.

Segundo Ofomaja, 2008, na maior parte dos casos a remoção de corantes aumenta com o aumento de massa de adsorvente, ou seja, ocorre o aumento do número de sítios de adsorção na área superficial do adsorvente, como demonstrado na Figura 5. Sendo assim, busca-se um ponto onde ocorra grande adsorção de corante com o mínimo de dosagem de corante.

Figura 5 – Efeito da dosagem de adsorvente na adsorção de corantes.

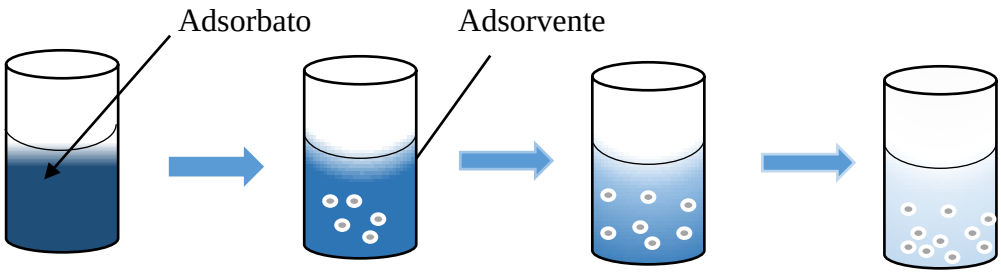

Fonte: Autor

3.10.2 Efeito do pH

O pH da solução é um dos parâmetros mais importantes para o processo de adsorção, devido a magnitude das cargas eletrostáticas transferidas pelas moléculas de corantes ionizadas ser controlada através do pH. De acordo com Salleh et al, 2011, geralmente em soluções de pH abaixo (se o meio estiver protonado ou dependendo do pKa do corante), ocorre a diminuição adsorção se o corante é catiônico e um aumento da adsorção se o corante for aniônico. Na Figura 6 está demonstrada o efeito do pH na adsorção de corantes (SALLEH et al., 2011).

Figura 6 - Efeito do pH na adsorção de corantes.

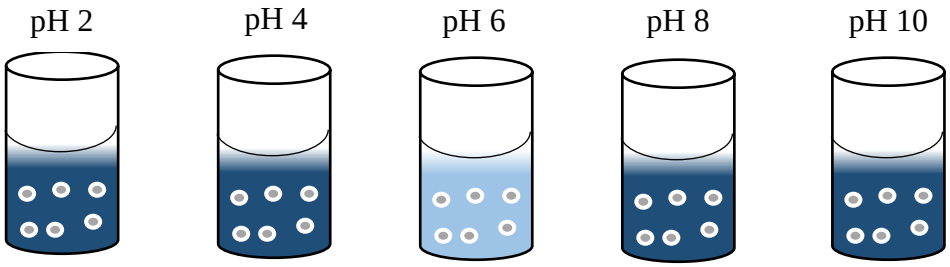

Fonte: Autor

3.10.3 Isotermas de Adsorção e Termodinâmica

Para descrever melhor como o adsorbato irá ser afetado pelo adsorvente, descrevendo assim a capacidade de adsorção podem ser utilizadas as isotermas de

adsorção, sendo que o principal modelo utilizado é a isoterma de Langmuir. De acordo com Rudzinski e Plazinki, 2007, o modelo de Langmuir baseia-se em um modelo monocamada ideal, levando em conta também que ocorre um processo de adsorção homogêneo em todos os sítios de adsorção (RUDZINSKI; PLAZINSKI, 2007). Outros modelos podem ser utilizados, como BET, Freundlich e Sips.

O efeito da temperatura é importante para indicar se a operação de adsorção é exotérmico ou endotérmico. Os processos endotérmicos possuem maior capacidade de adsorção com o aumento da temperatura, devido ao aumento do número de sítios ativos e de mobilidade em altas temperaturas. Em relação a processos exotérmicos, o aumento de temperatura acarreta na diminuição da capacidade de adsorção. (SENTHILKUMAAR; KALAAMANI; SUBBURAAM, 2006). Na Figura 7, está apresentado o efeito da mudança de temperatura na situação em que a transferência de calor é endotérmica. Com os dados da temperatura e os modelos ajustados é possível estimar os parâmetros termodinâmicos (ΔG°, ΔH°, ΔS°).

Figura 7 - Efeito da temperatura considerando a adsorção endotérmica

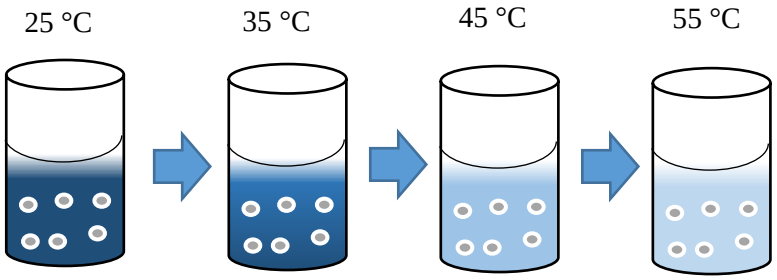

Fonte: Autor

3.10.5 Cinética de adsorção

O efeito do tempo de adsorção é estudado através da taxa de adsorção. De acordo com Seow e Lin, a taxa de adsorção é um importante fator para a escolha do material adsorvente, pois o material deve ter uma alta capacidade de adsorção e rápida taxa de adsorção. O principal modelo utilizado para descrever a cinética de adsorção é o pseudo-modelo de primeira ordem de Lagergren, criado em 1898. A partir deste foram criados outros modelos como o de pseudo-segunda ordem e de ordem n, sendo estes baseados no modelos que consideram a adsorção como uma reação química (HO; MCKAY, 1999). Além destes, existem outros tipos de modelos como o HSDM,

baseado na difusão do adsorbato nos poros (DOTTO; PINTO, 2012). Na Figura 8, está demonstrado a evolução da diminuição da concentração em relação ao tempo.

Figura 8 - Efeito do tempo na adsorção de corantes.

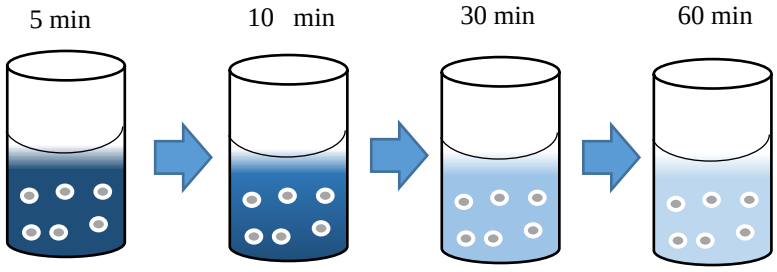

Fonte: Autor

4. NANO-SÍLICA OBTIDA DA CASCA DO ARROZ ATRAVÉS DE PROCESSO ALTERNATIVO COM ULTRASSOM E APLICAÇÃO PARA REMOÇÃO DE CORANTE

O artigo a seguir foi submetido a revista *Journal of Hazardous Materials* (ISSN: 0304-3894), Qualis A1 na área de Engenharias II.

Nano–silica obtained from rice husk through alternative sonication process and its application for dye removal

Enrique C. Peres[1], Jenifer Slaviero[1], André R. F. Almeida[2], Michele P. Enders[3], Edson I. Muller[3], Guilherme L. Dotto[1]*

[1]Chemical Engineering Department, Federal University of Santa Maria–UFSM, 1000 Roraima Avenue, 97105–900 Santa Maria, RS, Brazil.

[2]Chemical Engineering, Federal University of Pampa–UNIPAMPA, 1650 Maria Anunciação Gomes de Godoy street, 96413–170 Bagé, RS, Brazil.

[3]Department of Chemistry, Federal University of Santa Maria–UFSM, 1000 Roraima Avenue, 97105–900 Santa Maria, RS, Brazil.

ABSTRACT

Nano–SiO_2 was obtained from rice husk through an alternative ultrasound process, characterized and applied to remove Crystal Violet dye from aqueous media by adsorption. The better characteristics of ultrasound modified nano–silica (UM–$nSiO_2$) regarding to the standard nano–silica ($nSiO_2$) were demonstrated by infrared spectroscopy (FT–IR), X–ray diffraction (XRD), N_2 adsorption isotherms (BET and BJH methods), gas picnometry, differential scanning calorimetry (DSC) and scanning

electron microscopy (SEM). $nSiO_2$ and UM–$nSiO_2$ were used as adsorbents for Crystal Violet dye. The adsorption study was performed by kinetic curves, equilibrium isotherms and thermodynamics. UM–$nSiO_2$ presented significantly higher values of surface area, pore volume, pore diameter and porosity than $nSiO_2$. Pseudo–Second order model was the best for kinetic curves. To represent the equilibrium curves, BET and Freundlich were the most adequate. UM–$nSiO_2$ attained adsorption capacity of 495 mg g^{-1} coupled with removal percentage of 98%, being and excellent adsorbent for CV dye. For both adsorbents, the thermodynamic results revealed a favorable, spontaneous and endothermic process. These findings show that the ultrasound technique has great potential to intensify the silica production process, generating a material with better characteristics for dyes adsorption.

Keywords: Adsorption; Equilibrium; Nano–silica; Thermodynamics; Water.

4.1. INTRODUCTION

The search for alternatives to use solid wastes generated from agribusiness is a great challenge worldwide. The large generation of these materials, evidences the necessity for its management and valorization. Among these residues, it should be highlighted the generation of rice husk, rice straw, corn straw, which could be reused (AJMAL et al., 2003; GUO et al., 2017; SARKER; FAKHRUDDIN, 2015). The main use for rice husk is the burning for energy generation. As a result, residual ashes are also obtained. These ashes are basically composed by oxides, mainly silicon dioxide (SiO_2), which can be separated at high purity, if a suitable treatment is employed (XIONG et al., 2009). Silicon dioxide (SiO_2) is a semiconductor compound and due its physicochemical characteristics can be used in several sectors, such as, additive in concrete, manufacture of photovoltaic cells and manufacture of electronics (microchips and transistors) (LAZARO; QUERCIA; BROUWERS, 2012; WANG et al., 2003; WU et al., 2006). In general, silicon dioxide can be used in industrial processes like filtration (such filter aids), absorption and support in osmosis (TIAN et al., 2017; VANDER AUWERA et al., 2016; YUREKLI et al., 2017). In adsorption process, silicon dioxide can be utilized for heavy metals removal from aqueous media (FRANCO et al., 2017).

Silica can be obtained from rice husk by several routes. Four processes are more utilized: thermal, hydrothermal, biological or chemical treatment (BALABANOVA, 2003; CHESHMEH et al., 2013; GHORBANI; SANATI; MALEKI, 2015; POTAPOV et al., 2011). Among these processes, thermal treatment is the most used. This route is based on burning the feedstock at elevated temperatures (400 °C to 700 °C) to produce amorphous silica, followed by acid leaching for purification (SOLTANI et al., 2015). In this process, the acid leaching step has fundamental role, since is responsible for the elimination of metallic impurities such as iron (Fe), manganese (Mn), calcium (Ca), sodium (Na), potassium (K) and magnesium (Mg) that influence the purity and color of the silica. Furthermore, the physicochemical and textural characteristics of the obtained silica are affected by the leaching step. In this sense, the modification of production process, in the leaching step, utilizing different methods, such as ultrasound, can improve the characteristics of silica produced, as demonstrated with other materials in the literature (DOTTO et al., 2015; FRANCO et al., 2017). It is know that ultrasound treatment provokes extreme thermodynamic conditions at molecular level, which are able to modify the characteristics of the produced material (DOTTO et al., 2015; FRANCO et al., 2017).

The improvement of physicochemical characteristics of silica affects directly its application. Amorphous silica can be used to remove dyes from colored wastewater of textile industries by adsorption. Adsorption in turn, is one of the most common operations used to treat colored effluents, since is a cheap method and the adsorbent can be recovered (HARO et al., 2017). According to Weber and Chakravorti (WEBER; CHAKRAVORTI, 1974), we can still mention advantages like ease of operation and high potential to remove organic contaminants, including dyes.

In this work, it was proposed for the first time, the production of nano–SiO_2 using the thermal treatment of rice husk, followed by an alternative sonication process in the leaching step. For comparison, nano–SiO_2 was also produced by the standard process. This process modification aimed to improve the nano–SiO_2 characteristics like surface area, pore distribution, purity and mainly the potential to remove Crystal Violet dye (CV) from aqueous media by adsorption. The characteristics of ultrasound modified nano–silica (UM–nSiO_2) and standard nano–silica (nSiO_2) were investigated by infrared spectroscopy (FT–IR), X–ray diffraction (XRD), N_2 adsorption isotherms (BET and BJH methods), gas picnometry, differential scanning calorimetry (DSC) and scanning electron microscopy (SEM). For both materials (UM–nSiO_2 and nSiO_2), a detailed

evaluation of CV dye adsorption was performed, including the adsorbent dosage and pH effects, kinetic, equilibrium and thermodynamic studies.

4.2. MATERIALS AND METHODS

4.2.1. Obtainment and characterization of UM–$nSiO_2$ and $nSiO_2$

Rice husk (*Oryza Sativa*) was provided by a rice processing industry located in Santa Maria, RS, Brazil. Firstly, rice husk was washed with distilled water and oven dried (Solab, SL–101, Brazil) during 24 h at temperature of 50 ºC. After, rice rusk was burned in a furnace (Magnus, model 06 , Brazil) at 600 ºC during 6 h to remove the organic compounds and obtain the rice husk ashes (DAFFALLA; MUKHTAR; SHAHARUN, 2010). Then, the ashes were submitted to the leaching step using two ways:

- Standard leaching: rice husk ashes were put in contact with hydrochloric acid 10% w/w (HCl, Vetec, Brazil) (SOLTANI et al., 2015), and the solution was agitated in a magnetic stirrer (Marconi MA 093, Brazil) for 2 h at 80 °C.
- Sonication leaching: rice husk ashes were put in contact with hydrochloric acid 10% w/w (HCl, Vetec, Brazil) (SOLTANI et al., 2015), and the solution was submitted to sonication with a titanium sonotrode (UP200S, Hielscher, Germany), with frequency of 320 kHz, amplitude of 60%, temperature of 80 °C for 30 min.

After each leaching, samples were washed with deionized water and filtered (Whatmann n° 40). The samples were then dried during 24 h at 100ºC. To obtain nanometric particle size, the samples were macerated and put in a furnace at 700 °C with heating rate of 5 °C min^{-1} (SANKAR et al., 2016). The nano–SiO_2 prepared by the standard method was named $nSiO_2$ and the nano–SiO_2 prepared by the sonication method was named UM–$nSiO_2$.

The functional groups of the samples were confirmed by Fourier transform infrared spectroscopy (FT–IR) (Shimadzu, Prestige 21, Japan) in the range of 500–4500 cm^{-1}. X–ray powder diffractometry (XRD) (Rigaku, Miniflex 300, Japan), with Ni–filtered Cu Ka radiation (λ=1.54051 Å, 30 kV, 10 mA), with 2θ=5–100°, was employed to verify the samples crystallinity. The BET surface area, total pore volume and average pore radius of $nSiO_2$ and UM–$nSiO_2$ were obtained by N_2 adsorption isotherms at –196 °C (Micromeritcs, ASAP 2020, USA). Samples were pre–treated at 200 °C for 24 h under nitrogen atmosphere, in order to eliminate the moisture adsorbed on the solid surface. Samples were then submitted to 25 °C in vacuum, reaching the residual pressure of 10^{-4} Pa. The solid density was determined by helium gas picnometry (Ultrapyc, 1200e, Japan). The silica content in the samples was estimated by X–ray Fluorescence (XRF) (Shimadzu, Model EDX–720, Japan). The thermal profile of the samples were obtained by differential scanning calorimetry (DSC, TA Instruments, USA), from temperature 25 °C to 400 °C, under N_2 atmosphere. Scanning electron microscopy (SEM) (Jeol, JSM–6610LV, Japan) was utilized to analyze the textural characteristics of the samples.

4.2.2. Batch adsorption experiments

Methyl violet 10B (triarylmethane) or also know Crystal Violet (CV) was used as adsorbate in this work. CV ($C_{25}H_{30}ClN_3$, color index 42555, molar weight of 407.99 g mol^{-1}, λ_{max}=590 nm, purity above 95%) is a common cationic dye found in colored effluents of printing or paper industries (CHAKRABORTY et al., 2011). The Crystal Violet molecular structure, with the respective pK_a values is demonstrated in Figure 9

Figure 9 - Chemical structure of Crystal Violet dye.

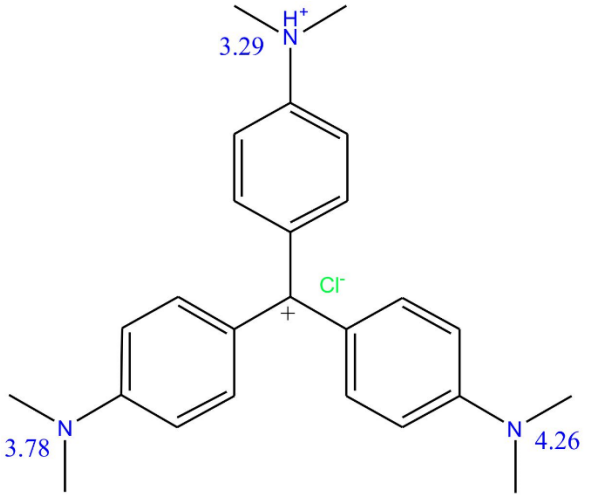

All experiments were performed in batch mode, at 220 rpm with solution volume of 50 mL, using a thermostated agitator (Marconi, MA 093, Brazil), aiming to evaluate the effects of adsorbent dosage, pH, equilibrium and kinetic curves. Firstly, CV stock solution (1.00 g L^{-1}) (INLAB, Brazil) was prepared, and then, the experiments were carried out by diluting the stock solution in distilled water. The adsorbent dosage effect was analyzed using 100, 250, 500, 750 and 1000 mg L^{-1} of $nSiO_2$ or UM–$nSiO_2$, with dye concentration of 50 mg L^{-1} at 25 °C for 4 h. The pH effect was studied in the same conditions, but using pH of 2, 4, 6, 8, 10 and the pre−determined adsorbent dosage. Equilibrium curves were constructed in the more adequate adsorbent dosage and pH, with initial concentrations of Crystal Violet 50, 100, 200, 300, 400 and 500 mg L^{-1}, at temperatures of 25, 35, 45 and 55 ºC (the equilibrium was considered after three consecutive equal measurements of dye concentration in liquid phase). Kinetic curves were constructed with contact time from 0 to 240 min, for initial CV concentrations of 50, 100, 200 and 300 mg L^{-1}, in the best pH and adsorbent dosage. For all adsorption tests, the solid phase was separated by centrifugation and the Crystal Violet concentration was determined by UV–vis spectrometry (Shimadzu, UV–1800, model). The experiments were realized in replicate (n=3) and blanks were performed. Eqs. (1) and (2) were used to determine the equilibrium adsorption capacity (q_e) and the adsorption capacity at time 't' (q_t), respectively:

$$q_e = \frac{C_0 - C_e}{m} V \qquad (1)$$

$$q_t = \frac{C_0 - C_t}{m} V \quad (2)$$

where, C_0 is the initial concentration of Crystal Violet (mg L^{-1}), C_t is the CV concentration at time 't' (mg L^{-1}), C_e is the equilibrium concentration (mg L^{-1}), m is the adsorbent amount (g), and V is the volume of solution (L).

4.2.3. Kinetics and isotherms

Pseudo–first order (LANGMUIR, 1918a) and Pseudo–second order (HO; MCKAY, 1999) models were utilized to compare the CV adsorption on $nSiO_2$ and UM–$nSiO_2$. It is know that these models consider adsorption as a chemical reaction without take into account the mass transfer steps, but, the models are mathematically simpler and are able to compare adsorption capacities. Pseudo–first order model (Eq. (3)) was proposed by Lagergren's, reporting the liquid–solid adsorption systems (LAGERGREN, 1898).

$$q_t = q_1(1 - \exp(-k_1 t)) \quad (3)$$

where, k_1 is the rate constant of Pseudo–first order (min^{-1}) and q_1 is the theoretical value of adsorption capacity (mg g^{-1}).

Pseudo–second order model (Eq. (4)) has better performance for long contact times (HO; MCKAY, 1999). One relevant parameter studied is the Pseudo–second order is the initial sorption rate h_0 (mg g^{-1} min^{-1}), presented in Eq. (5) (HO et al., 2004; UNUABONAH; ADEBOWALE; OLU-OWOLABI, 2007):

$$q_t = \frac{t}{(1/k_2 q_2^{\,2}) + (t/q_2)} \quad (4)$$

$$h_0 = k_2 q_2^2 \quad (5)$$

being, k_2 the rate constant of Pseudo–second order model (g mg^{-1} min^{-1}) and q_2 the theoretical value of adsorption capacity (mg g^{-1}).

BET and Freundlich isotherms were used to fit the equilibrium data. The choice of these models was based on the type of equilibrium curves obtained for the systems CV/nSiO_2 and CV/UM–nSiO_2. The BET model for solid–liquid adsorption is represented by the Eq. (6) (EBADI; SOLTAN MOHAMMADZADEH; KHUDIEV, 2009):

$$q_e = \frac{q_{BET} k_S C_e}{(1 - k_L C_e)(1 - k_L C_e + k_S C_e)} \quad (6)$$

where, q_{BET} is the monolayer adsorption capacity (mg g^{-1}), k_s and k_L are the BET constants (L mg^{-1}).

Freundlich isotherm is another multilayer model utilized (INGLEZAKIS; POULOPOULOS, 2006). The Freundlich isotherm is represent by Eq. (7) (FREUNDLICH, 1906):

$$q_e = k_F C_e^{1/nF} \quad (7)$$

where, k_F is Freundlich constant (mg g^{-1})(mg L^{-1})$^{-1/nF}$ and $1/n_F$ is the heterogeneity factor.

In relation to the parameters estimation, all parameters were calculated through nonlinear regression, using Quasi–Newton method in Statistic 10.0 software (Statsoft, USA), fitting the kinetic and equilibrium models. Average relative error (ARE) and coefficient of determination (R^2) were used to compare the results.

4.2.4. Thermodynamic parameters estimation

Generally, to understand the effect of temperature in the adsorption, some parameters are estimated such as: the standard entropy change (ΔS^0, kJ mol^{-1} K^{-1}), standard Gibbs free energy change (ΔG^0, kJ mol^{-1}) and standard enthalpy change (ΔH^0, kJ mol^{-1}) (AMMENDOLA; RAGANATI; CHIRONE, 2017). Standard Gibbs free energy was calculated to determine the spontaneity of adsorption process. Furthermore,

ΔS^0 and ΔH^0 are others parameters of feasibility, representing the organization of adsorbate molecules and the adsorption heat, respectively. ΔS^0, ΔG^0 and ΔH^0 were estimated by Eqs. (8) and (9):

$$\Delta G^o = -RT\ln(K^o) \tag{8}$$

$$\ln(K^o) = \frac{\Delta S^o}{R} - \frac{\Delta H^o}{RT} \tag{9}$$

where, R is universal constant (kJ $mol^{-1}K^{-1}$), T is temperature (K) and K^o is the thermodynamic constant (dimensionless). For each adsorption system, K^o was estimated from the parameters of the best fit equilibrium model.

4.3. RESULTS AND DISCUSSION

4.3.1. Nano–silica characteristics

The FT–IR spectra of $nSiO_2$ and UM–$nSiO_2$ are depicted in Figures 10 (a) and 10 (b), respectively. Both spectra were similar, presenting the same vibrational bands as follows: 3430 cm^{-1} relative to O–H or SiO–H stretching's and 1635 cm^{-1} relative to the H–O–H vibration (possibly due the presence of H_2O molecules on the surface). The vibrational bands related with the presence of silicon dioxide are presented at 1080, 800 and 460 cm^{-1}. The asymmetric stretching vibrations of Si–O–Si can be observed at 1080 cm^{-1}). The Si–O–Si symmetric stretching vibrations were found at 800 cm^{-1}. The band at 474 cm^{-1} is relative to the O–Si–O bending vibrations (AL-OWEINI; EL-RASSY, 2009; MUSIĆ; FILIPOVIĆ-VINCEKOVIĆ; SEKOVANIĆ, 2011). These results show that all produced samples ($nSiO_2$ and UM–$nSiO_2$) are relatively pure (since no strange bands were found).

Figure 10 – FT–IR spectra of (a) $nSiO_2$ and (b) UM–SiO_2.

a)

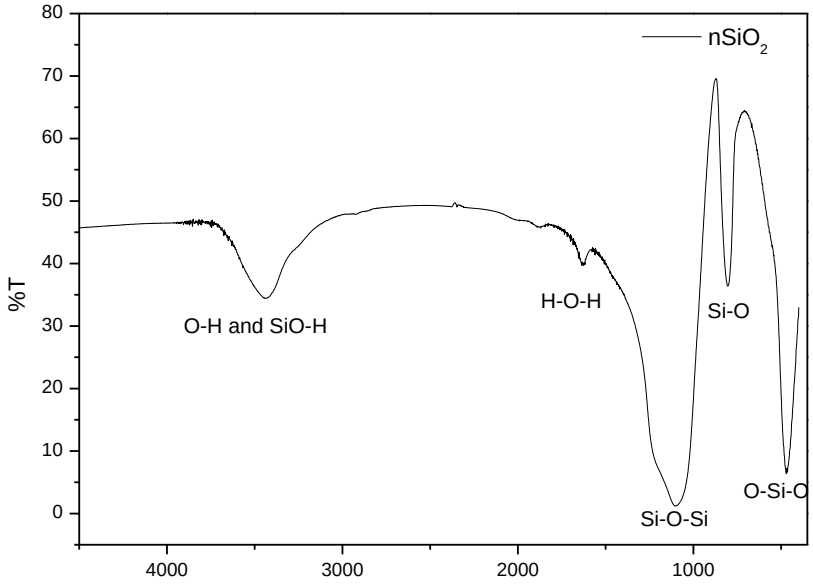

b)

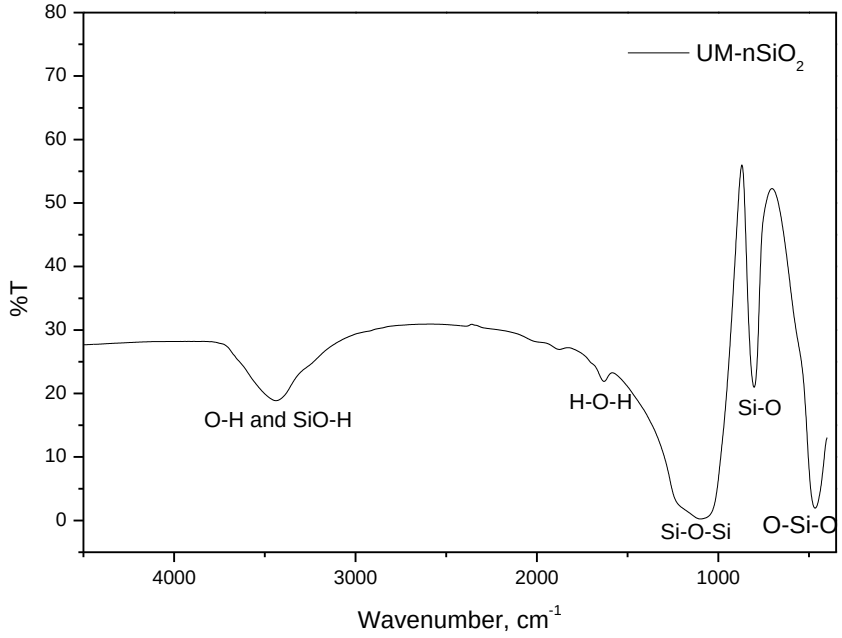

The XRD patterns of $nSiO_2$ and UM–$nSiO_2$ are show in Figure 11. Both patterns were similar and the profile was typical of amorphous silica. This is in accordance with the literature, since to obtain crystalline SiO_2, temperatures over 700 °C are required (SARANGI; BHATTACHARYYA; BEHERA, 2009), and in this work we used 700 °C as upper limit.

Figure 11 - XRD patterns of $nSiO_2$ and $UM–SiO_2$.

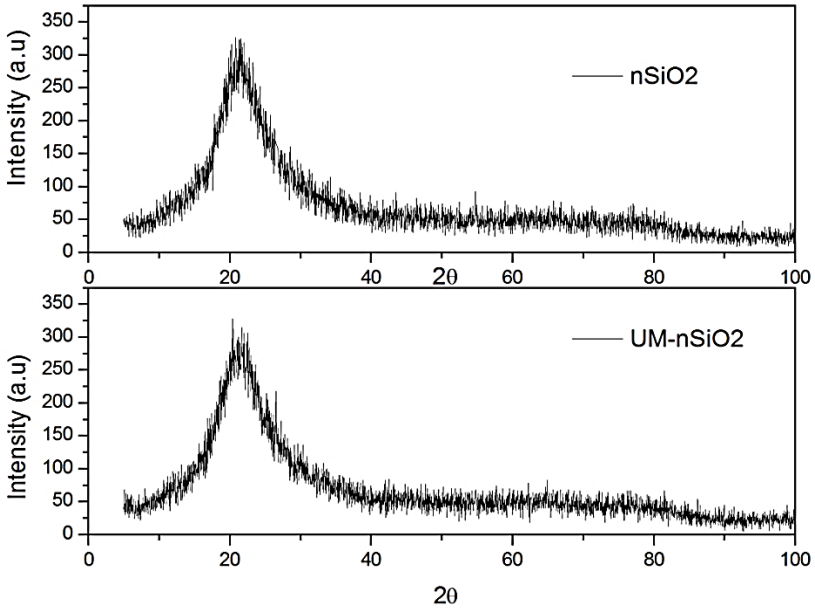

The N_2 adsorption–desorption isotherms of $nSiO_2$ and $UM–nSiO_2$ are shown in Figures 12 (a) and 12 (b), respectively. Both materials presented the same isotherm profile, with a hysteresis loop. This behavior is typical of mesoporous solids [29]. Normally, inorganic oxides compounds, such as silicon dioxide, are classified as mesoporous solids (YUE; ZHOU, 2008). The pore size distribution is depicted in Figure 13. From this Figure, it is possible confirm that $nSiO_2$ and $UM–nSiO_2$ are mesoporous materials (pore diameter mainly concentrated in the range from 2 to 50 nm). Furthermore, it is possible verify that $UM–nSiO_2$ presented more distributed pore volume in the mesoporous region while, for $nSiO_2$, a peak centered at around 9 nm was observed.

Figure 12 – N_2 adsorption–desorption isotherms of (a) $nSiO_2$ and (b) $UM–SiO_2$.

a)

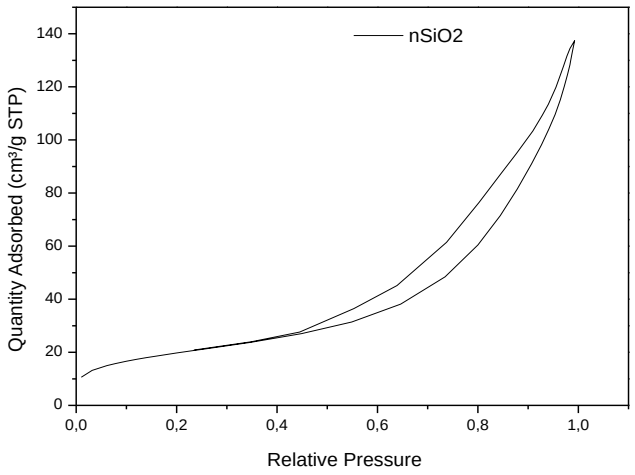

b)

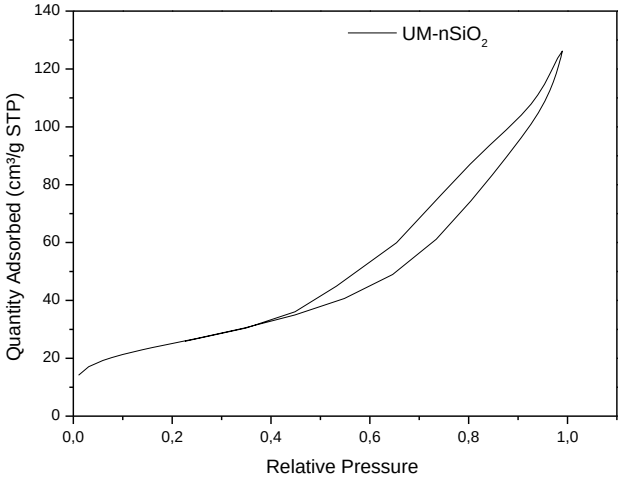

Figure 13 - Pore size distribution of $nSiO_2$ and $UM–SiO_2$.

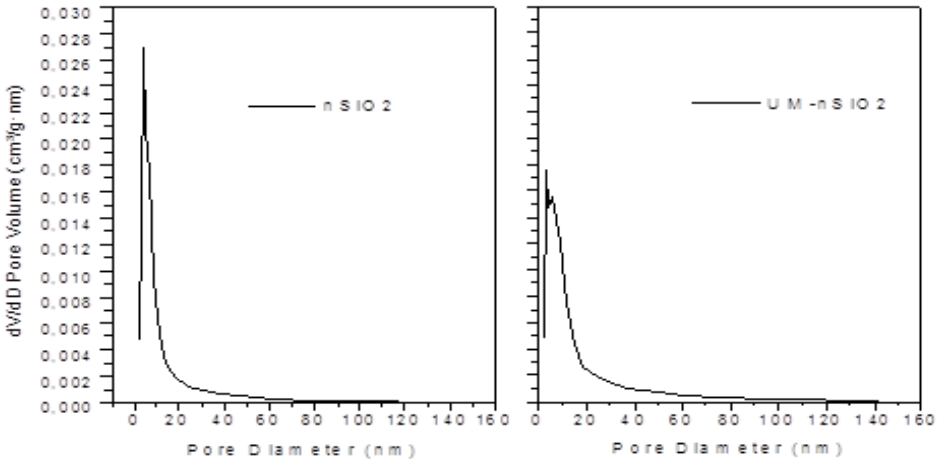

The characteristics of $nSiO_2$ and UM–SiO_2 determined by BET, BJH, X–ray fluorescence and gas picnometry are shown in Table 2. It can be seen that UM–SiO_2 presented surface area 30% higher than $nSiO_2$. The total pore volume, average pore diameter and porosity were also higher for UM–SiO_2. UM–SiO_2 resented also higher solid density and purity than $nSiO_2$. Higher values of surface area, pore volume, pore diameter and porosity are required for adsorption purposes, since allow the transference of the adsorbate molecules inside of the adsorbent. Also, are responsible for more available binding sites. The higher values of solid density confirm the higher purity of UM–SiO_2 in relation to the $nSiO_2$. For comparison, Sankar et al. prepared nanosilica from three types of rice husk ashes (sticky, red and brown). They found surface areas of 7.5, 201.4 and 247.1 $m^2\ g^{-1}$, respectively [21]. In the work of Ghorbani et al. amorphous nanosilica with average particle size of 200 nm and purity of 97% was obtained from rice husk [15].

Table 2 - Characteristics of $nSiO_2$ and UM–SiO_2 determined by BET, BJH, X–ray fluorescence and gas picnometry.

	$nSiO_2$*	UM–$nSiO_2$*
BET Surface Area ($m^2\ g^{-1}$)	71.97±0.43	91.05±0.25
Total volume of pores ($cm^3\ g^{-1}$)	0.200±0.002	0.216±0.001
Average pore diameter (nm)	8.4±0.2	11.2±0.3
ρ_s ($g\ cm^{-3}$)	2.712±0.053	3.431±0.021
Porosity	0.35±0.02	0.43±0.01
Purity (%)	97.8±0.1	99.5±0.1

mean±standard error for 3 measurements.

Differential scanning calorimetry (DSC) was utilized to interpret the thermal data of $nSiO_2$ and UM–$nSiO_2$. The results are shown in Figure 14 and Table 3. Figure 14 (a) ($nSiO_2$) shows an endothermic peak at 74.74 ºC with ΔH^0 of 0.0932 J g^{-1} (Table 3), which is relative to the water evaporation. The water evaporation peak was also observed for UM–$nSiO_2$, but at 61.15 ºC (Figure 14 (b)) with ΔH^0 of 0.0521 J g^{-1}. This shows that the water evaporation was easier in UM–$nSiO_2$, probably due the favorable textural characteristics (pore volume, pore diameter, porosity and surface area) above presented. Furthermore, for $nSiO_2$, a second endothermic peak was verified at 250.35 ºC, which is relative to desorption of chlorine ions. Thus occurs because $nSiO_2$ presented poor textural characteristics in relation to UM–$nSiO_2$, and the chloride ions

can remain impregnated in the pores, even after the washings and conventional leaching.

Figure 14 - DSC curves of (a) $nSiO_2$ and (b) $UM–SiO_2$.

a)

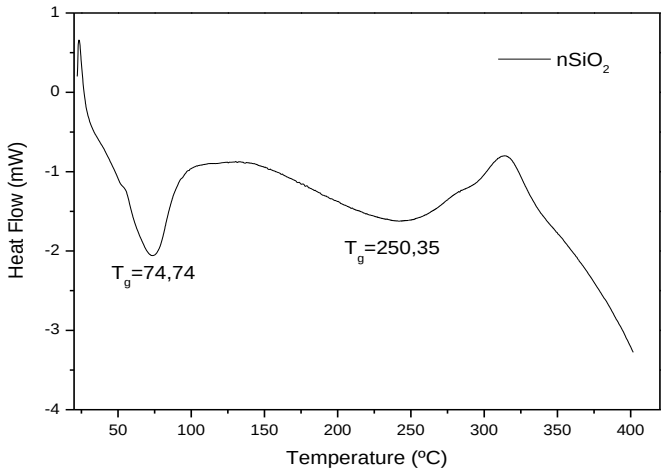

b)

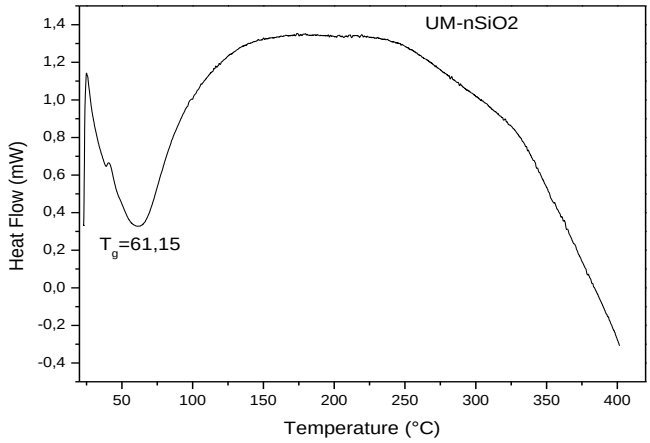

Table 3 - Differential scanning calorimetry data for $nSiO_2$ and $UM–SiO_2$.

Sample	Peak	ΔH^0 (J g^{-1})	Process
$nSiO_2$	First	0.0932	Water evaporation
	Second	0.2279	Dessorption of chorine ions
$UM–nSiO_2$	First	0.0521	Water evaporation

The SEM images of $nSiO_2$ and $UM–nSiO_2$ at 50,000× of magnification are presented in Figures 15 (a) and 15 (b), respectively. It is possible verify that for $nSiO_2$

larger particles remained after the silica production. For UM–nSiO_2, an agglomerate of nanoparticles with diameter lower than 200 nm can be observed (Figure 15 (b)).

Figure 15 - – SEM images of (a) nSiO_2 and (b) UM–SiO_2.

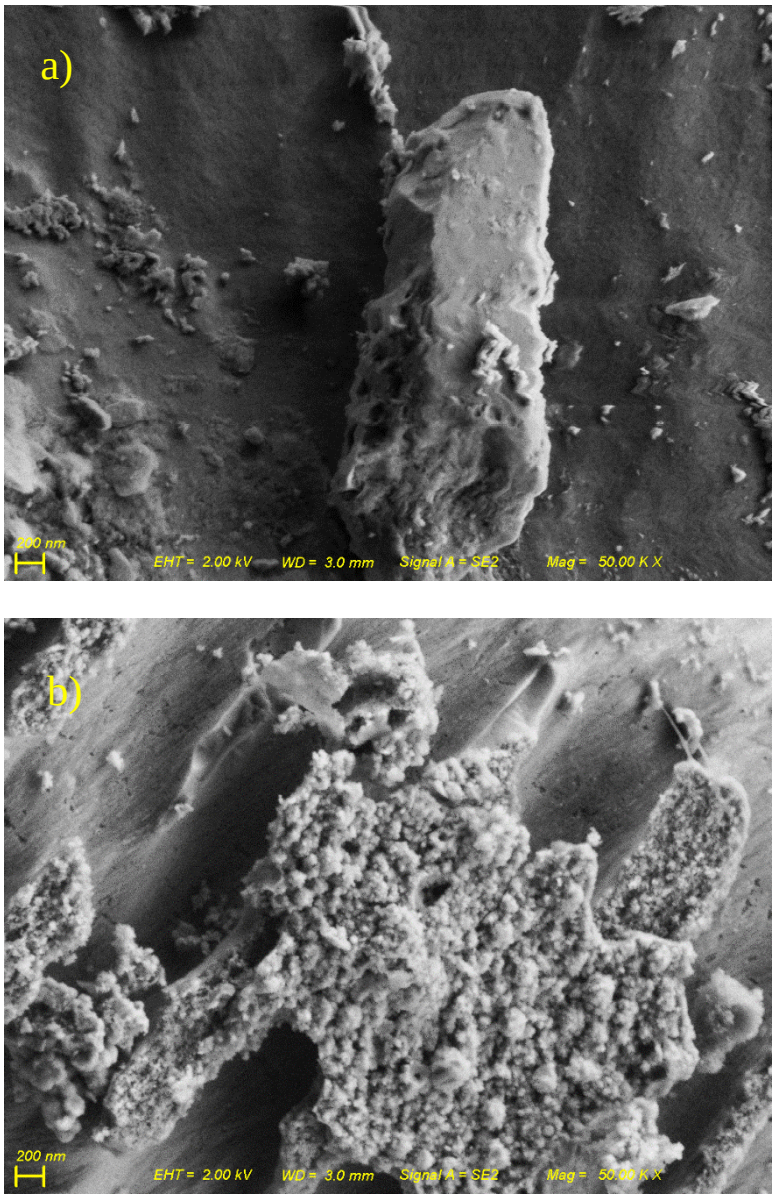

Based on the characterization techniques including FT–IR, XRD, N_2 adsorption isotherms, gas picnometry, XRF, DSC and SEM, we can affirm that UM–nSiO_2 presented better characteristics than nSiO_2 for adsorption purposes. Both materials were amorphous and presented typical functional groups of silica. However, UM–nSiO_2 presented higher surface area, pore volume, pore diameter, density, porosity and purity than nSiO_2. On the light of these results, it is clear that the alternative sonication process is able to produce a high quality and purity nano–SiO_2. The possible explanation for these better characteristics of UM–nSiO_2 is the hot spot theory. During the alternative

sonication leaching, cavities were formed on the liquid, under extreme thermodynamic conditions and, the implosion of these cavities released liquid jets at high velocities, leading to modifications into the silica characteristics. It is know that sonication process in liquids generates acoustic cavitation (generating microbubbles and shock waves), that cause the creation of microjets in heterogeneous liquids (SODIPO; AZIZ, 2018). Furthermore, a mechanical stirring was created due the collapse of microbubbles and shock wave's effect.

4.3.2. Adsorbent dosage effect on Crystal Violet adsorption

The adsorbent dosage effect on the CV removal was evaluated using 100, 250, 500, 750 and 1000 mg L^{-1} of $nSiO_2$ or UM–$nSiO_2$, with dye concentration of 50 mg L^{-1} at 25 °C for 4 h. The results are shown in Figure 16. For both materials, the adsorbent dosage increase caused an increase in the CV removal percentage. This occurs because there are more adsorption sites to interact with the dye molecules (PENG et al., 2015). Also, it can be seen that until 250 mg L^{-1} of adsorbent dosage, the removal percentage was the same for both adsorbents. However, from 250 to 1000 mg L^{-1}, UM–$nSiO_2$ presented higher removal percentage. Removal percentages around 90% were found using 1000 mg L^{-1} of UM–$nSiO_2$. Based on these results, the subsequent studies were performed using adsorbent dosage of 1000 mg L^{-1}.

Figure 16 - Adsorbent dosage effect on CV adsorption by (■) $nSiO_2$ and (●) $UM–SiO_2$ (C_0=50 mg L^{-1}, 25 °C, 4 h).

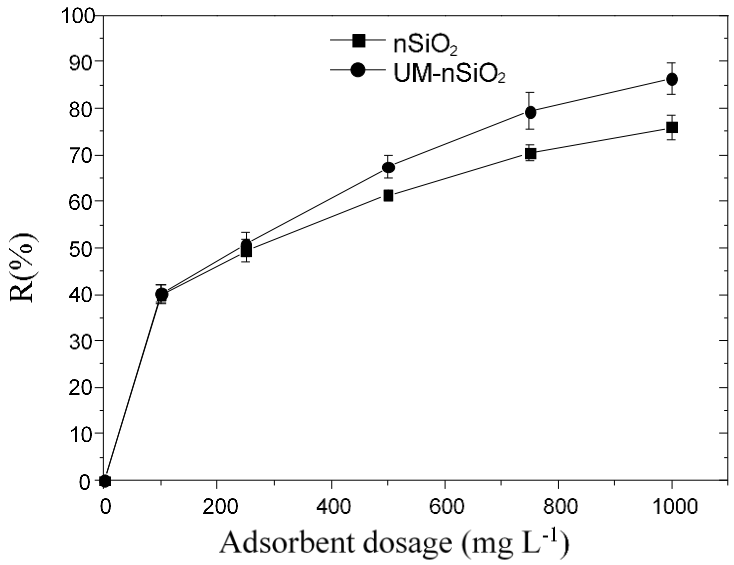

4.3.3. pH effect on Crystal Violet adsorption

pH is one of the most important factors regarding dyes adsorption, since affects the functional groups located on the adsorbent surface and the ionization degree of the dye molecules (FERREIRA et al., 2011). Here, the pH effect was evaluated from of 2 to 10 with dye concentration of 50 mg L^{-1} at 25 °C for 4 h. Results are presented in Figure 17. Both adsorbents presented similar results regarding to the pH effect. The adsorption capacity increased with the pH increase, being the best results obtained at pH of 10. This occurred because at low pH values, there is a competition between the H^+ ions in solution with the CV cationic dye to occupy the adsorption sites. When the pH is increased, this competition decreases and consequently, the CV adsorption capacity is higher (AHMAD, 2009). In this way, the subsequent experiments were realized using pH of 10.

Figure 17 - pH effect on CV adsorption by (●) $nSiO_2$ and (■) UM–SiO_2 (C_0=50 mg L^{-1}, 25 °C, 4 h, adsorbent dosage of 1000 mg L^{-1}).

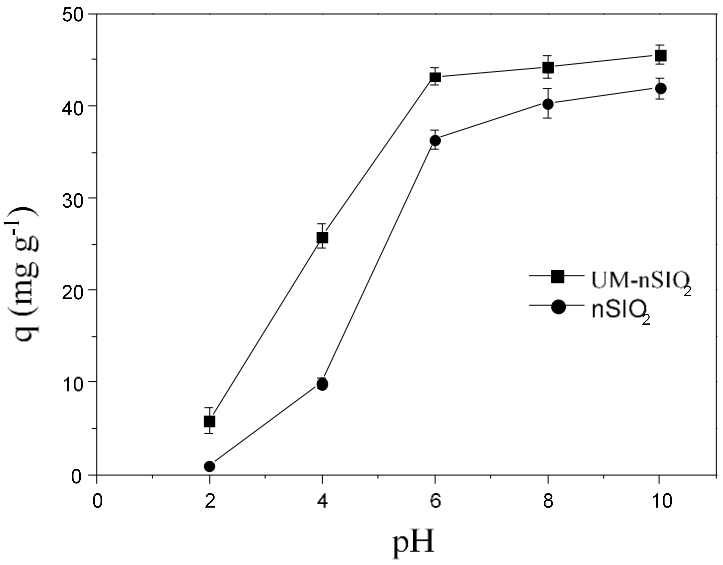

4.3.4. Kinetic studies

For both adsorbents, kinetic curves were constructed with contact time from 0 to 240 min, for initial CV concentrations of 50, 100, 200 and 300 mg L^{-1}, using adsorbent dosage of 1000 mg L^{-1} at pH of 10. Figure 18 shows the kinetics curves for the CV adsorption onto $nSiO_2$ and UM–$nSiO_2$. In relation to the stirring time, for all concentrations, it was possible remove 80% of the dye within 60 min. Furthermore, the data proved a fast adsorption. Another important factor is the high adsorption capacity, mainly obtained at high dye concentrations.

Adsorption kinetics was investigated by the Pseudo–first order and Pseudo–second order models. All kinetic parameters for the CV adsorption on $nSiO_2$ and UM–$nSiO_2$ are shown in Table 4. Pseudo–second order model was the more adequate to represent the adsorption kinetics of $nSiO_2$ and UM–$nSiO_2$, since presented high values of coefficient of determination (R^2>0.97) and low values of average relative error (ARE<7.00%) (Table 4). For both materials, q_2 increased with the initial dye concentration, confirming that the adsorption capacity is favored at higher values of C_0. For all conditions, q_2 values for UM–$nSiO_2$ were higher than q_2 values for $nSiO_2$. At initial concentrations of 300 mg L^{-1} UM–$nSiO_2$ presented adsorption capacity 15%

higher. In the same way, the h_0 values were higher for UM–$nSiO_2$, demonstrating that, at the initial stages, the amount of CV adsorbed by UM–$nSiO_2$ was higher than $nSiO_2$.

The kinetic studies revealed that UM–$nSiO_2$ is a better adsorbent for CV than $nSiO_2$, since presented higher values of adsorption capacities and faster adsorption rate. This result can be explained on the basis in the different characteristics of the materials. UM–$nSiO_2$ presented higher surface area, pore volume, pore diameter and porosity than $nSiO_2$. As consequence, the CV mass transfer was facilitated and more adsorption sites were available, leading to higher adsorption capacities and faster adsorption rates.

Table 4 - Kinetic parameters for the Crystal Violet adsorption on $nSiO_2$ and UM–SiO_2.

Kinetic models	Dye concentration (mg L^{-1})							
	$nSiO_2$				UM–$nSiO_2$			
	50	100	200	300	50	100	200	300
Pseudo–First Order								
q_1 (mg g^{-1})	37.2	73.9	166.3	231.7	38.3	79.3	171.6	269.9
k_1 (min^{-1})	1.55	24.07	0.56	1.76	1.96	1.22	1.87	2.14
R^2	0.9591	0.9523	0.9415	0.9633	0.9545	0.9344	0.9784	0.9870
ARE (%)	6.81	7.22	8.43	6.02	6.49	8.78	4.66	3.51
Pseudo–Second Order								
q_2 (mg g^{-1})	38.7	79.5	172.7	239.8	39.6	83.3	176.7	276.0
k_2 (g mg min^{-1})	0.0698	0.0259	0.00605	0.0134	0.0905	0.0227	0.0217	0.0190
h_0 (mg g min^{-1})	104.5	164.1	180.5	771.2	142.1	157.7	680.7	1448.0
R^2	0.9836	0.9849	0.9819	0.9835	0.9722	0.9742	0.9932	0.9957
ARE (%)	3.99	3.58	4.34	4.07	5.16	5.01	2.44	2.00

Figure 18 - Kinetic curves for Crystal Violet adsorption on (a) $nSiO_2$ and (b) $UM–SiO_2$ (25 °C, pH of 10, adsorbent dosage of 1000 mg L^{-1}).

a)

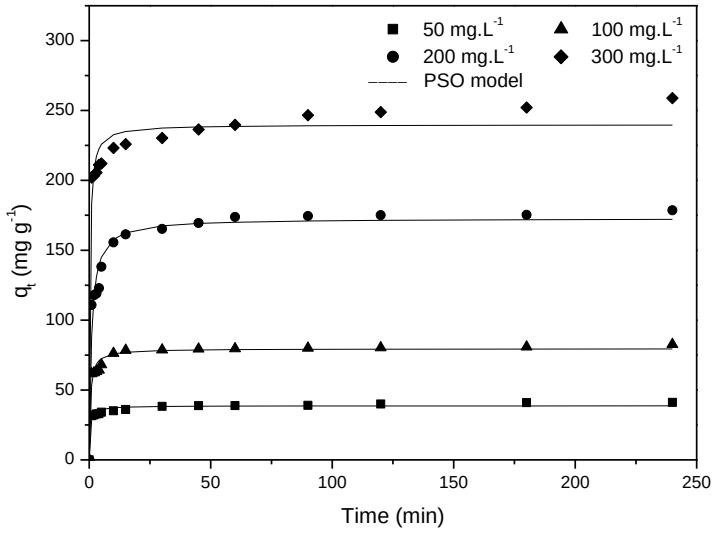

b)

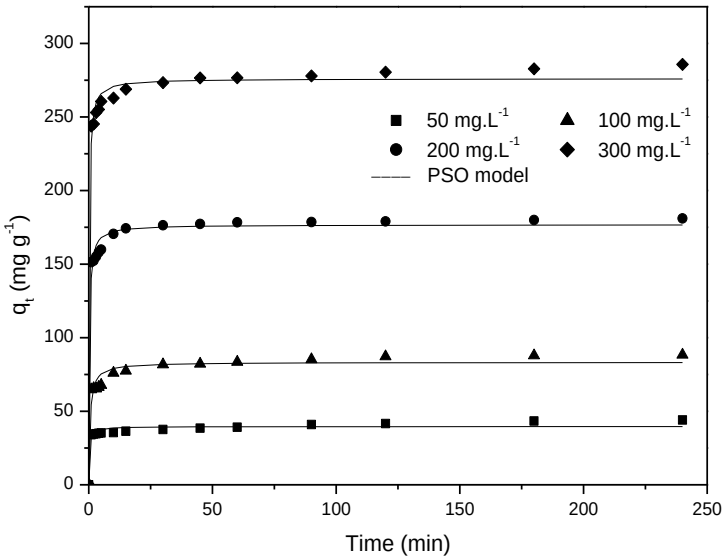

4.3.5. Equilibrium results

The equilibrium isotherms for CV adsorption on $nSiO_2$ and $UM–nSiO_2$ are presented in Figures 19 (a) and 19 (b), respectively. All curves can be classified as 'S' curves (vertical orientation isotherms) (GILES et al., 1958). It can be seen that the adsorption was favored by the temperature decrease. Also, higher removal percentages were found even at higher initial dye concentrations. For example, at 328 K, the CV

remaining concentration in liquid phase was lower than 5 mg L^{-1}, which represents removal percentages higher than 95%.

Based on the curves shape, BET and Freundlich models were selected to represent the CV adsorption on both adsorbents. The results are shown in Table 5. For $nSiO_2$, the BET model presented higher values of coefficient of determination (R^2>0.98) and lower values of average relative error (ARE<15.00%). The parameter k_L increased with the temperature indicating that the adsorption is favored at 328 K. The other parameters presented no clear trends. For UM–$nSiO_2$, the Freundlich model presented higher values of coefficient of determination (R^2>0.99) and lower values of average relative error (ARE<16.00%). The parameter k_F increased with the temperature indicating that the adsorption is also favored at 328 K.

Since BET and Freundlich models were used, it was not possible perform a comparison using the common maximum adsorption capacity from the Langmuir model. So, the maximum experimental values were used. In this work, UM–$nSiO_2$ attained adsorption capacity of 495 mg g^{-1} coupled with removal percentage of 98%, being and excellent adsorbent for CV dye. Brião et al. (BRIÃO et al., 2017) obtained maximum adsorption capacities for CV of 141.8 and 1217.3 mg g^{-1} using ZSM–5 and chitin/ZSM–5 zeolites, respectively. Sarma et al. (PARAB et al., 2006) studied the adsorption of Crystal violet on raw and acid treated montmorillonite, and found adsorption capacities of 370.37 and 400.00 mg g^{-1}, respectively. Kulkarni et al. (KULKARNI et al., 2017) studied the adsorption of Crystal Violet dye from aqueous solution using water hyacinth and found adsorption capacity of 322.58 mg g^{-1}. Mango stone biocomposite was prepared by Shoukat et al. (SHOUKAT et al., 2016) and was employed for the adsorption of Crystal Violet dye. The process variables were optimized and the maximum dye adsorption was 352.79 mg g^{-1}.

Based on the above results, it can be affirmed that the UM–$nSiO_2$ prepared in this work, is an excellent adsorbent to remove CV from aqueous media. UM–$nSiO_2$ presents the intrinsic characteristics of silica, like thermal, mechanical and chemical resistance, coupled with fast adsorption kinetics, high adsorption capacity and high dye removal percentage.

Figure 19 – Equilibrium curves for Crystal Violet adsorption on (a) $nSiO_2$ and (b) $UM–SiO_2$ (pH of 10, adsorbent dosage of 1000 mg L^{-1}).

a)

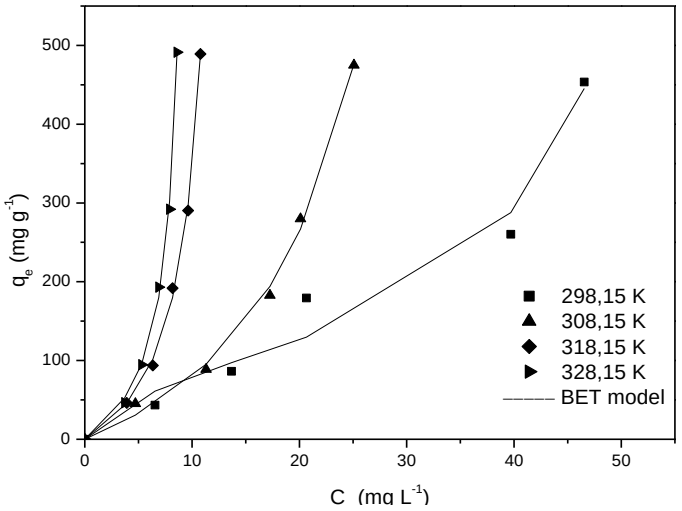

b)

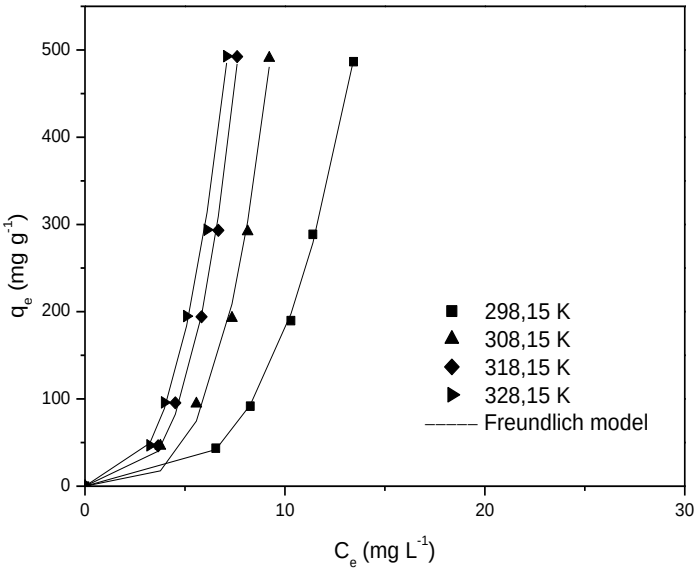

Table 5 - Equilibrium parameters for the Crystal Violet adsorption on $nSiO_2$ and $UM–SiO_2$.

Models	Temperature (K)							
	$nSiO_2$				$UM–nSiO_2$			
	298	308	318	328	298	308	318	328
BET								
k_S	0.1548	0.0208	0.0706	0.1415	0.0559	0.4289	0.2381	0.1490
k_L	0.0167	0.0264	0.0752	0.1010	0.0688	0.0896	0.1043	0.1032
q_{BET} (mg g^{-1})	102.1	266.2	115.2	71.90	153.2	88.32	112.0	164.6
R^2	0.9866	0.9982	0.9992	0.9990	0.9613	0.9628	0.9643	0.9692
ARE (%)	14.60	8.58	2.96	4.21	35.3	30.9	33.2	31.5
Freundlich								
k_F (mg g^{-1})(mg L^{-1})$^{-}_{1/nf}$	4.19E–11	2.03E–05	0.1779	0.0981	0.0692	0.1292	0.4927	1.5702
$1/n_F$	0.1277	0.1892	0.3017	0.2541	0.2931	0.2701	0.2945	0.3414
R^2	0.7713	0.8721	0.9925	0.9878	0.9995	0.9949	0.9984	0.9981
ARE (%)	58.70	50.6	15.81	18.41	2.10	15.21	5.84	4.50

4.3.6. Thermodynamics results

The thermodynamic parameters (ΔG^0, ΔH^0 and ΔS^0) were estimated for both adsorption systems, and the results are demonstrated in Table 6. The Kº values (dimensionless thermodynamic constant) were estimated from the isotherm parameters as recently reported in literature [45,46]. Table 6 shows that the Crystal Violet adsorption processes using $nSiO_2$ and $UM–nSiO_2$ were spontaneous and favorable, since the ΔG^0 values were negative. The positive ΔH^0 values demonstrated that both adsorption processes were endothermic. From the magnitude of ΔH^0 it is possible infer about the interactions that occurs between the adsorbent and adsorbate. Physisorption, such as van der Waals interactions, are usually lower than 20 kJ mol^{-1}, and electrostatic interaction ranges from 20 to 80 kJ mol^{-1}. Chemisorption bond strengths can be from 80 to 450 kJ mol^{-1} [46]. In this way, we can understand that electrostatic interactions between Crystal Violet and nano–SiO_2 materials have occurred. The electrostatic interactions are also corroborated by the pH effect (section 3.3). The positive ΔS^0 values

suggest the possibility of some structural changes or readjustments in the CV–adsorbent complex. In relation to the Crystal Violet adsorption, Kulkarni et al. (KULKARNI et al., 2017) found similar thermodynamic parameters using water hyacinth as adsorbent.

Table 6 - Thermodynamic parameters for the Crystal Violet adsorption on nSiO2 and UM–SiO2.

Adsorbent	T (K)	ΔG^0 (kJ mol^{-1})*	ΔH^0 (kJ mol^{-1}) *	ΔS^0 (kJ mol^{-1} K^{-1}) *
$nSiO_2$	298.15	–6.84±0.12	25.6±0.7	0.09±0.01
	308.15	–4.38±0.10		
	318.15	–5.54±0.05		
	328.15	–6.33±0.04		
$UM–nSiO_2$	298.15	–5.32±0.11	31.2±1.2	0.12±0.02
	308.15	–9.31±0.12		
	318.15	–8.68±0.06		
	328.15	–8.73±0.15		

*Mean ± standard error for n=3.

4.4. CONCLUSION

In this work, an alternative sonication process was proposed to obtain nano–silica from rice husk. Nano–silica was prepared by conventional ($nSiO_2$) and alternative sonication ($UM–nSiO_2$) processes. Both materials were characterized and used as adsorbents to remove Crystal Violet dye from aqueous media by adsorption. The results revealed that, compared to the conventional process, the alternative sonication process was able to produce a higher quality nano–silica, with particle size lower than 200 nm. Both materials ($nSiO_2$ and $UM–nSiO_2$) were amorphous and presented typical functional groups of silica. The material prepared by sonication process ($UM–nSiO_2$) presented surface area 30% higher than the material prepared by the conventional process ($nSiO_2$). The pore volume, pore diameter, density, porosity and purity were also higher for $UM–nSiO_2$.

The Crystal Violet adsorption using $nSiO_2$ and $UM–nSiO_2$ was favored with adsorbent dosage of 1000 mg L^{-1} and pH of 10. The kinetic curves were adequately represented by Pseudo–second order model. BET and Freundlich equilibrium models were able to fit the CV adsorption on $nSiO_2$ and $UM–nSiO_2$, respectively. In general, the potential of $UM–nSiO_2$ to adsorb CV was 15% higher in relation to $nSiO_2$. $UM–nSiO_2$ reached adsorption capacity of 495 mg g^{-1} coupled with removal percentage of 98%. In brief, it can be stated that $UM–nSiO_2$ prepared by the alternative sonication

process, is an excellent adsorbent to remove CV from aqueous media, since presents the intrinsic characteristics of silica, like thermal, mechanical and chemical resistance, coupled with fast adsorption kinetics, high adsorption capacity and high dye removal percentage.

ACKNOWLEDGEMENTS

The authors would like to thank CAPES (Brazilian Agency for Improvement of Graduate Personnel) and CNPq (National Council of Science and Technological Development) for the financial support.

5. SÍNTESE DE NANO-PARTÍCULAS DE SÍLICA ATRAVÉS DE MICRO-ONDAS E APLICAÇÃO NA ADSORÇÃO DO CORANTE AZUL DE METILENO.

O artigo a seguir está publicado na revista *Journal of Environmental Chemical Engineering* (ISSN: 22133437) (Volume 6, Issue 1, February 2018, Pages 649–659), Qualis B1 na área de Engenharias II.

Microwave synthesis of silica nanoparticles and its application for methylene blue adsorption

Enrique C. Peres[1], Jenifer C. Slaviero[1], Anaelise M. Cunha[1], Ahmad Hosseini–Bandegharaei[2], Guilherme L. Dotto[1]*

[1]Chemical Engineering Department, Federal University of Santa Maria–UFSM, Santa Maria, RS, Brazil.

[2]Wastewater Division, Faculty of Health, Gonabad University of Medical Sciences, PO Box 119, Gonabad, Iran.

ABSTRACT

Silica nanoparticles were obtained from rice husk through an alternative microwave process and applied to remove Methylene Blue dye (MB) from aqueous media by adsorption. The better characteristics of microwave modified nano–silica (MW–$nSiO_2$) regarding to the standard nano–silica ($nSiO_2$) were demonstrated by X–ray diffraction, infrared spectroscopy, N_2 adsorption isotherms, gas picnometry, differential scanning calorimetry and scanning electron microscopy. $nSiO_2$ and MW–$nSiO_2$ were used as adsorbents to remove MB dye from aqueous media. The adsorption study was performed by kinetic curves, equilibrium isotherms and thermodynamics. MW–$nSiO_2$

presented higher values of surface area, pore volume, pore diameter and porosity than $nSiO_2$. Pseudo–n order and HSDM models were adequate to represent the kinetic profile. To represent the equilibrium curves, the Sips model was the most adequate. MW–$nSiO_2$ attained adsorption capacity of 679.9 mg g^{-1} coupled with removal percentage of 80%, being and excellent adsorbent for MB dye. For both adsorbents, the thermodynamic results revealed a favorable, spontaneous and exothermic process. These findings show that microwave is a powerful technique to intensify the silica production process, generating a material with better characteristics for dyes adsorption.

Keywords: Adsorption; Methylene blue; Microwave; Nanoparticles; Silica.

5.1. INTRODUCTION

Large amounts of agricultural wastes are produced every day in the world, generating a great environmental problem, due to the lack of management purposes in the industrial sector. Wastes derived from corn, rice and wheat are generate in large quantities, and consequently, studies have been performed in order to obtain interesting routes to enjoy these solid wastes (MA; ZHAO; DIAO, 2016; MALIK, 2003; TAN et al., 2012). Rice husk is a typical example of agricultural wastes, and normally, is burned in the boilers to generate energy (UEASIN; LIAO; WONGCHAI, 2015). Rice husk is composed by organic and inorganic fractions. Among the organic compounds are lignin, cellulose and hemicellulose. In relation to the inorganic compounds, silicon oxide (SiO_2) is the most abundant, being normally obtained through rice husk burning (MA'RUF; PRAMUDONO; ARYANTI, 2017). During the rice husk burning, ashes are generated, and these requires additional processes such as leaching or organosolv (ROSA et al., 2016) to obtain SiO_2 and then, add value for this waste.

Silicon dioxide (SiO_2) is largely used in the industry, since is a semiconductor with high chemical resistance. Silica nanoparticles in turn, is a material generated from SiO_2, containing interesting characteristics, which enables several applications. In environmental area, the effect of nanosilica to decrease the salinity stress on plants was investigated (ABDEL-HALIEM et al., 2017). Furthermore, nanosilica is utilized to improve the resistance, durability and flame resistance of cements (FANGLONG et al., 2016). The production of silica nanoparticles already presents improvements with respect to silica, but, it is still possible modify the nanosilica characteristics through

alternative processes, such as microwave, ultrasound or oxidative processes, in order to improve the potential of this material (FRANCO et al., 2017).

The study of different processes to improve the silica characteristics is relevant, since the physicochemical characteristics affect directly the application [9,10]. An example is the application of silica based materials in adsorption processes (FRANCO et al., 2017). Adsorption is a very common operation used to treat colored effluents containing Methylene blue (MB), a typical dye, highly toxic, utilized in textile, paper and pesticides industries (CHEN et al., 2017). Nanoparticles of amorphous silica can be used to remove MB dye from colored wastewaters of textile industries by adsorption. In this sense, the modification of the preparation route can enhance the adsorption properties of the silica nanoparticles.

The main objective of this research was the preparation of silica nanoparticles from rice husk, using the microwave technology in the leaching step, aiming the improvement of surface area, pore distribution, purity and Methylene Blue adsorption capacity (MB). The microwave modified nano–silica (MW–nSiO_2) and standard nano–silica (nSiO_2) were prepared and characterized by X–ray diffraction (XRD), infrared spectroscopy (FT–IR), N_2 adsorption isotherms (BET and BJH), gas picnometry, differential scanning calorimetry (DSC) and scanning electron microscopy (SEM). For both materials, adsorption kinetic, equilibrium and thermodynamic aspects were investigated.

5.2. MATERIALS AND METHODS

5.2.1 Obtainment and characterization of nSiO_2 and MW–nSiO_2

Rice husks (*Oryza sativa L.*) were provided by a rice processing industry located in Santa Maria, RS, Brazil. Rice husks were washed with distilled water and oven dried (Solab, SL–101, Brazil) during 24 h at 50 °C. In next step, rice rusks were burned in a furnace (Magnus, model 06 , Brazil) at 600 °C during 6 h, to remove the organic compounds and obtain the rice husk ashes [15]. The ashes were then submitted to the leaching step using two ways:

→ Standard leaching: rice husk ashes were put in contact with hydrochloric acid 10% w/w (HCl, Vetec, Brazil), and the solution was agitated in a magnetic stirrer (Marconi MA 093, Brazil) for 2 h at 80 °C;

→Microwave leaching: rice husk ashes were put in contact with hydrochloric acid 10% w/w (HCl, Vetec, Brazil), and the solution was submitted to heating of microwaves (CEM, Mars 6, Japan) with temperature of 80 °C for 30 min.

After leaching, the samples were washed with deionized water and filtered (Whatmann n° 40). The materials were dried during 24 h at 100 °C. To obtain nanometric particle size, the samples were macerated and put in a furnace at 700 °C with heating rate of 5 °C min^{-1} (SANKAR et al., 2016). The material prepared by the standard method was named $nSiO_2$, and the material obtained by the microwave leaching was named MW–$nSiO_2$.

The characteristics of $nSiO_2$ and MW–$nSiO_2$ were assessed by X–ray diffraction (XRD), infrared spectroscopy (FT–IR), N_2 adsorption isotherms (BET and BJH), gas picnometry, differential scanning calorimetry (DSC) and scanning electron microscopy (SEM). The samples crystallinity was verified through X–ray powder diffractometry (XRD) (Rigaku, Miniflex 300, Japan), with Ni–filtered Cu Ka radiation (λ=1.54051 Å, 30 kV, 10 mA), using 2θ=5–100°; Fourier transform infrared spectroscopy (FT–IR) (Shimadzu, Prestige 21, Japan) was used to identify the functional groups of the samples in the range of 500–4500 cm^{-1}; Total pore volume, average pore radius, pore size distribution and surface area were obtained by N_2 adsorption isotherms at –196 °C (Micromeritcs, ASAP 2020, USA). Samples were pre–treated at 200 °C for 24 under nitrogen atmosphere, in order to eliminate the moisture adsorbed on the solid surface. Samples were then submitted to 25 °C in vacuum, reaching the residual pressure of 10^{-4} Pa. BET and BJH methods were used to obtain the characteristics; The solid density was determined by helium gas picnometry (Ultrapyc, 1200e, Japan); DSC (differential scanning calorimetry) (DSC, TA Instruments) was utilized to determine the thermal profile of the samples; Scanning electron microscopy (SEM) (Jeol, JSM–6610LV, Japan) was used to analyze the textural characteristics of the samples.

Figure 20 - Chemical structure of Methylene Blue dye.

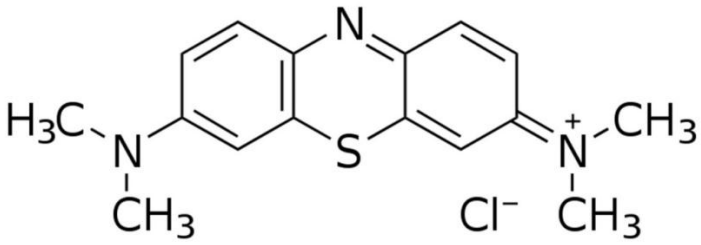

5.2.2. Adsorption experiments

All adsorption experiments were carried out by diluting a stock of solution of Methylene Blue (MB) (Fig. 20) (color index 52015, molar weight of 319.8 g mol^{-1}, λ_{max} = 664 nm, pKa = 5.6) (1.00 g L^{-1}) in distilled water. The experiments were realized in batch operation using a thermostated agitator (Marconi, MA 093, Brazil). The tests of adsorbent dosage, pH, equilibrium and kinetic were performed. For all tests, the stirring rate was 250 rpm and the volume solution was 50 mL.

The adsorbent dosage effect was evaluated using 100, 250, 500, 750 and 1000 mg L^{-1} of $nSiO_2$ and MW–$nSiO_2$, with dye concentration of 50 mg L^{-1} at 298 K, during 4 h. The pH effect was studied using pH values of 2, 4, 6, 8 and 10, after the determination of adsorbent dosage, with dye concentration of 50 mg L^{-1} at 298 K, during 4 h. Kinetic curves were constructed (more adequate values of adsorbent dosage and pH), with a contact time ranging from 0 to 240 min, for initial dye concentrations of 50, 100, 200 and 300 mg L^{-1} at 298 K. The equilibrium curves were generated using initial dye concentrations of 50, 100, 200, 300 and 500 mg L^{-1}, with temperatures of 298, 308, 318 and 328 K. After the experiments, the solid/liquid separation was performed by filtration (Whatmann n° 40). The quantification of Methylene Blue in liquid phase was realized by UV–vis spectrometry (UV–mini, Shimadzu, Japan) at 664 nm. The tests were realized in replicate (n=3) and blanks were performed. Eqs. (1) and (2) were utilized to determine the equilibrium adsorption capacity (q_e) and the adsorption capacity at time 't' (q_t), respectively:

$$q_e = \frac{C_0 - C_e}{m} V \tag{1}$$

$$q_t = \frac{C_0 - C_t}{m} V \tag{2}$$

where, C_0 is the initial MB concentration in liquid phase (mg L^{-1}), C_t is the MB concentration in liquid phase at time 't' (mg L^{-1}), C_e is the equilibrium MB

concentration in liquid phase (mg L^{-1}), m is the adsorbent amount (g), and V is the volume of solution (L).

5.2.3. Kinetic and isotherms

To adjust the kinetic data, four different models were used: pseudo−first order, pseudo−second order, pseudo−n−order and HSDM (Homogeneous solid diffusion model). Pseudo−first order (PFO) (LANGMUIR, 1918b), pseudo−second order (PSO) (HO; MCKAY, 1999) and pseudo−n−order (PNO) (G. RITCHIE, 1977) are commonly utilized, and consider adsorption as a reaction. These models are presented in Eqs. (3), (4) and (5), respectively:

$$q_t = q_1(1-\exp(-k_1 t)) \tag{3}$$

$$q_t = \frac{t}{(1/k_2 q_2{}^2) + (t/q_2)} \tag{4}$$

$$q_t = q_n - \frac{q_n}{\left[k_n (q_n)^{n-1} t(n-1)+1\right]^{\frac{1}{(n-1)}}} \tag{5}$$

being, k_1, k_2 and k_n the rate constants of pseudo–first order, pseudo–second order and pseudo−n−order models, respectively, in (min^{-1}) and (g mg^{-1} min^{-1}) and (min^{-1}(g mg^{-1})$^{n-1}$); q_1, q_2 and q_n are the theoretical values for the adsorption capacity (mg g^{-1}) and n is the reaction order.

Homogeneous solid diffusion model (HSDM) was also employed in this work, to find preliminary information regarding the mass transfer aspects. This model is utilized for spherical and amorphous particles, where, a unidirectional and isothermal transference occurs. In addition, intraparticle diffusion is considered the rate limiting step (DOTTO; PINTO, 2012; QIU et al., 2009; RUTHVEN, 1984; SONETAKA et al., 2009). HSDM model is presented in Eq. (6), and its initial and boundary conditions are presented in Eqs. (7), (8) and (9):

$$\frac{dq}{dt} = \frac{1}{r^2}\frac{d}{dr}\left(r^2 D_{int}\frac{dq}{dr}\right) \tag{6}$$

$$q(r,0) = 0 \tag{7}$$

$$q(R_p, t) = q_e \tag{8}$$

$$\left(\frac{dq}{dr}\right)_{r=0} = 0 \tag{9}$$

Considering the intraparticle diffusivity (D_{int}, $cm^2\ s^{-1}$) as a constant value, and long adsorption times (Fourier number higher than 0.2), Crank found a solution for HSDM model as presented in Eq. (10) (CRANK, 1979):

$$\frac{q_t}{q_e} = 1 - \left[\frac{6\alpha(\alpha-1)\exp\left(-\frac{q_n^2 D_{int} t}{R_p^2}\right)}{9 + 9\alpha + q_n^2\alpha^2}\right] \tag{10}$$

where D_{int} is the intraparticle diffusion coefficient ($cm^2\ s^{-1}$), r is the radial position (cm), q is the adsorbed quantity in the solid (mg g^{-1}) varying with radial position at time, R_p is the particle radius (cm), α is the effective volume ratio, expressed as a function of the equilibrium partition coefficient (solid/liquid concentration ratio) ($C_e/(C_0 - C_e)$) and q_n represent the roots other than zero of Eq. (11):

$$\tan q_n = \frac{3q_n}{3 + \alpha q_n^2} \tag{11}$$

To estimate the equilibrium parameters, three models were utilized: Langmuir, Freundlich and Sips. Langmuir is the most utilized, since contains physical assumptions such as, each site can contain only one adsorbate molecule and adsorption occurs in a monolayer (LANGMUIR, 1918b). The Langmuir model is represented by Eq. (12):

$$q_e = \frac{q_m k_L C_e}{1 + (k_L C_e)} \tag{12}$$

where, q_m is the maximum adsorption capacity (mg g^{-1}) and k_L is the Langmuir constant (L mg^{-1}).

The Freundlich isotherm is a heterogeneous model utilized when the amount adsorbed increase infinitely with the concentration (FREUNDLICH, 1906). The Freundlich isotherm is represent by Eq. (13):

$$q_e = k_F C_e^{1/nF} \tag{13}$$

where, k_F is the Freundlich constant ($mg^{1-c}L^c g^{-1}$), where $c=1/n_F$) and $1/n_F$ is the heterogeneity factor.

The Sips model is a combination of Langmuir and Freundlich models, and can be expressed in the form of Eq. (14) (SIPS, 1948):

$$q_e = \frac{q_{mS}(k_S C_e)^m}{1+(k_S C_e)^m} \tag{14}$$

where, q_{mS} is the maximum adsorption capacity of Sips (mg g^{-1}), k_S is the Sips constant (L mg^{-1}) and m is the fractional exponent.

Kinetic and equilibrium parameters were calculated through nonlinear regression of the experimental data, using Quasi–Newton method in Statistic 10.0 software (Statsoft, USA). The fit quality was evaluated by the average relative error (ARE), coefficient of determination (R^2), adjusted determination coefficient (R^2_{adj}) and Akaike information criterion (AIC)

5.2.4. Adsorption thermodynamics

Standard Gibbs free energy change (ΔG^0, kJ mol^{-1}), standard enthalpy change (ΔH^0, kJ mol^{-1}) and standard entropy change (ΔS^0, kJ mol^{-1} K^{-1}) were used to interpret the adsorption thermodynamics. These values were estimated from Eq. (15) [26]:

$$\Delta G^0 = -RT\ln(K) = \Delta H^0 - T\Delta S^0 \tag{15}$$

where, R is the universal constant (kJ mol^{-1} K^{-1}), T is temperature (K) and K is the standard thermodynamic constant (dimensionless), which was obtained from the parameters of the best fit isotherm model.

5.3. RESULTS AND DISCUSSION

5.3.1. $nSiO_2$ and MW–$nSiO_2$ characteristics

XRD patterns of $nSiO_2$ and MW–$nSiO_2$ are presented in Fig. 21. Both samples presented typical structure of amorphous silicon, with the characteristic peak at 2θ=22°. This is in accordance with the literature (SANKAR et al., 2016), which relates that amorphous silica is normally obtained when temperatures below 800 °C are used. For dye adsorption purposes, amorphous materials are more adequate, since this type of structure can better accommodate these large molecules.

Figure 21- XRD patterns of $nSiO_2$ and MW–$nSiO_2$.

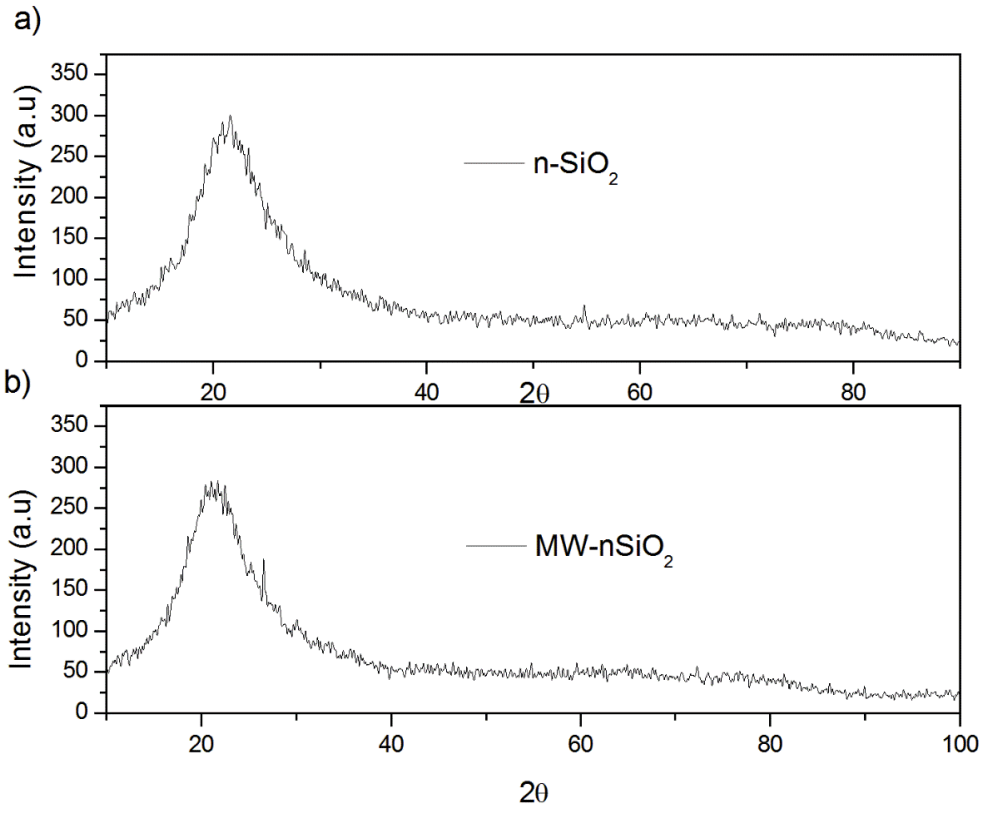

Fourier transform infrared spectroscopy (FT–IR) was utilized to identify the main functional groups on the samples surface. FT–IR spectra of $nSiO_2$ and MW–$nSiO_2$ are presented in Fig. 22a and 22b, respectively. Both materials presented similar FT–IR spectrum, with the main bands at 3430, 1635, 1080, 800 and 460 cm^{-1}. The band at 3430 cm^{-1} represents the vibrations of O–H or SiO–H groups. The IR band at 1635 cm^{-1}

is relative to the H–O–H vibration, suggesting the presence of H_2O molecules in the sample. The IR bands related with silicon dioxide can be visualized at 1080 cm^{-1} (Si–O–Si asymmetric stretching vibration), 800 cm^{-1} (Si–O–Si symmetric stretching vibration) and 460 cm^{-1} (O–Si–O bending vibration) (MESTANZA et al., 2017). In general, it was found that, for both materials, the bands presented similar wavenumber and intensity. This behavior indicates that no chemical bonds were formed or destructed as consequence of the microwave application. Only physical modifications occurred. Finally, the identified groups can be potential adsorption sites to uptake MB dye from aqueous media.

Figure 22 - FT–IR spectra of (a) $nSiO_2$ and (b) MW–$nSiO_2$.

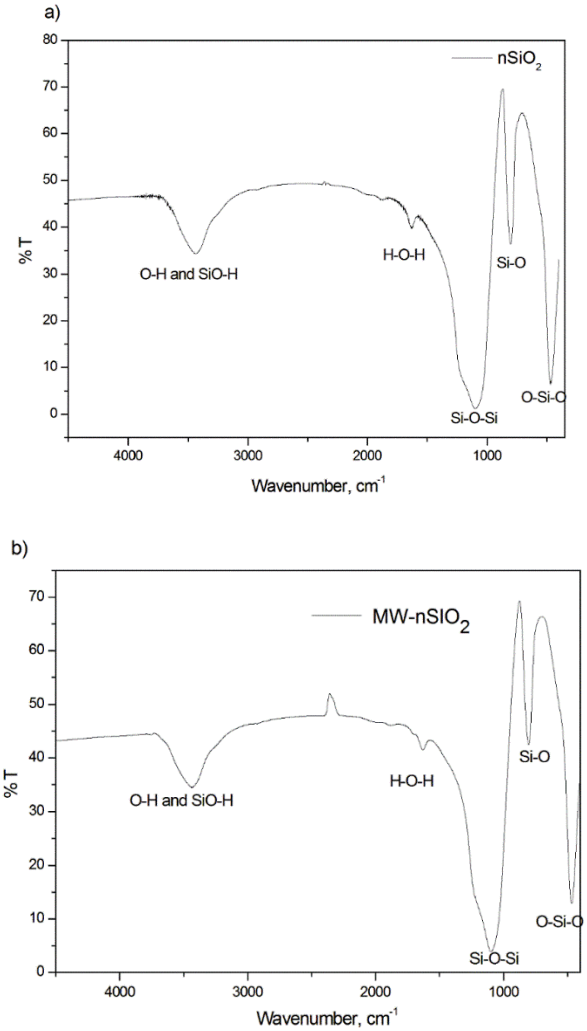

The N_2 adsorption/desorption isotherms of $nSiO_2$ and MW–$nSiO_2$ are presented in Fig. 23. For both materials the isotherms were similar and typical of mesoporous solids, presenting a hysteresis loop. Inorganic oxides compounds, such as silicon

dioxide, are classified, in general, as mesoporous solids (YUE; ZHOU, 2008). Moreover, BJH was utilized for determine the pore size distribution as show in Fig. 24. Both samples are mesoporous materials (porous in the range from 2 to 50 nm). The characteristics of $nSiO_2$ and MW–$nSiO_2$ determined by BET, BJH, X–ray fluorescence and gas picnometry are presented in Table 7. It can be seen that the material prepared by microwave (MW–$nSiO_2$) presented better characteristics than the standard material ($nSiO_2$), in terms of surface area, pore volume and average pore diameter. Furthermore, the porosity of MW–$nSiO_2$ was evidently higher. The values of density and purity were also higher for the material prepared by microwave. The better characteristics of MW–$nSiO_2$ are adequate for dyes adsorption purposes, since more dye molecules can occupy the void spaces on the material structure.

Table 7 - Characteristics of $nSiO_2$ and MW–$nSiO_2$ determined by BET, BJH, X–ray fluorescence and gas picnometry.

	$nSiO_2$	MW–$nSiO_2$
BET Surface Area ($m^2\ g^{-1}$)	71.97 ± 0.43	84.56 ± 0.23
Total volume of pores ($cm^3\ g^{-1}$)	0.2005 ± 0.0020	0.2218 ± 0.0025
Average pore diameter (nm)	8.44 ± 0.21	9.84 ± 0.11
ρ ($g\ cm^3$)	2.712 ± 0.053	3.260 ± 0.061
Porosity	0.352 ± 0.022	0.418 ± 0.034
Purity (%)	97.8 ± 0.1	98.8 ± 0.1

mean±standard error for 3 measurements.

Figure 23 - N_2 adsorption–desorption isotherms of (a) $nSiO_2$ and (b) $MW–nSiO_2$.

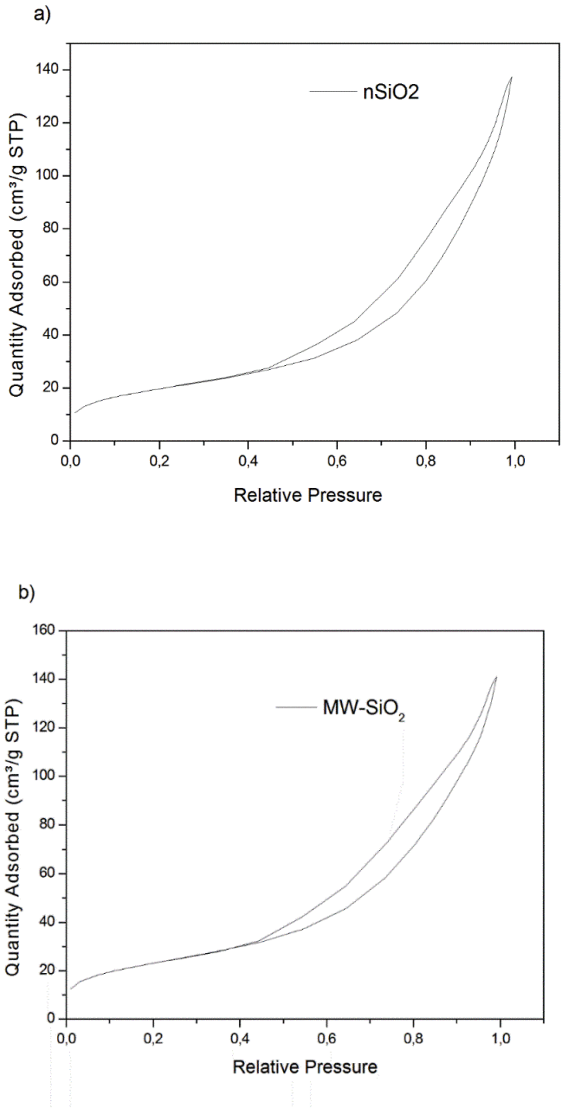

Figure 24 - Pore size distribution of $nSiO_2$ and $MW–nSiO_2$.

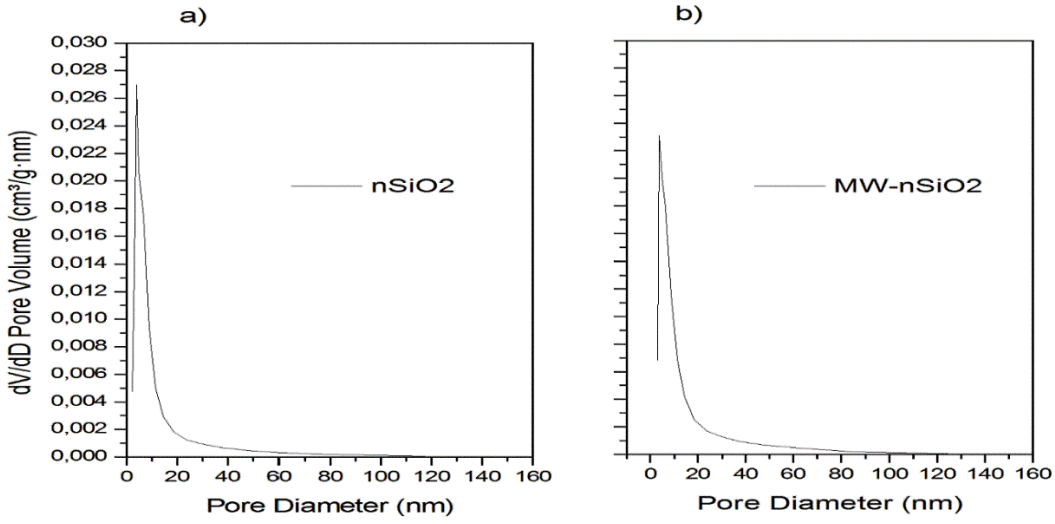

The thermal data of both materials were analyzed through differential scanning calorimetry (DSC). Fig. 25a and Fig. 25b, present the DSC curves of $nSiO_2$ and MW–$nSiO_2$, respectively. Both DSC curves presented a peak of water evaporation. However the peaks were at temperature at 74.74 ºC and 43.80 °C for of $nSiO_2$ and MW–$nSiO_2$, respectively. Also, the enthalpy variation regarding the water evaporation was lower for MW–$nSiO_2$ (Table 8). These findings reveal that water evaporation was easier for MW–$nSiO_2$. This occurred because this material presented higher values of pore size, pore volume and porosity, facilitating the water transference inside the material. A peak centered at around 250 °C was found in $nSiO_2$ (Fig. 25a), indicating the degradation of residual materials, which were not removed during the conventional process preparation. On the other hand, this peak was not verified for MW–$nSiO_2$ (Fig. 25b), indicating that the microwave process was more efficient to provides a high purity material.

Table 8 - Differential scanning calorimetry data for $nSiO_2$ and MW–$nSiO_2$.

Sample	$\Delta H°$ (J g^{-1})	Process
$nSiO_2$	0.0932	Water evaporation
MW–$nSiO_2$	0.0463	Water evaporation

Figure 25 - DSC curves of (a) $nSiO_2$ and (b) MW–$nSiO_2$.

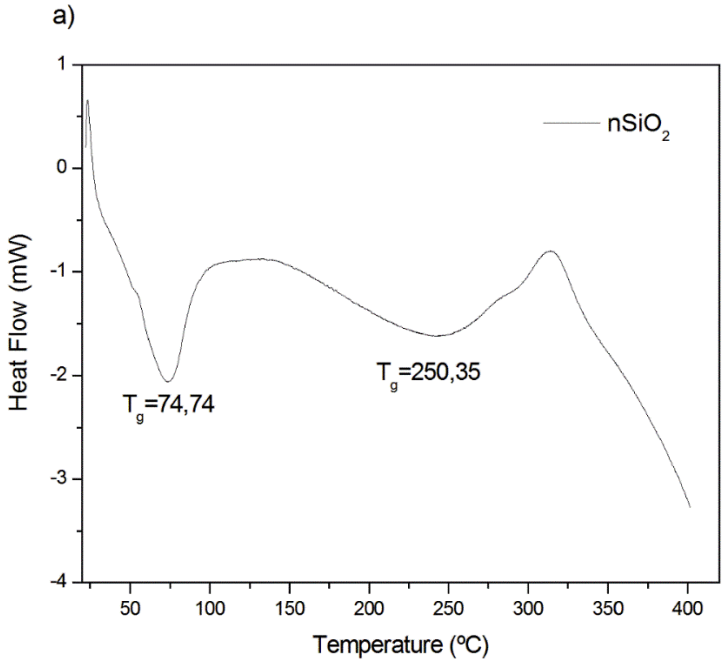

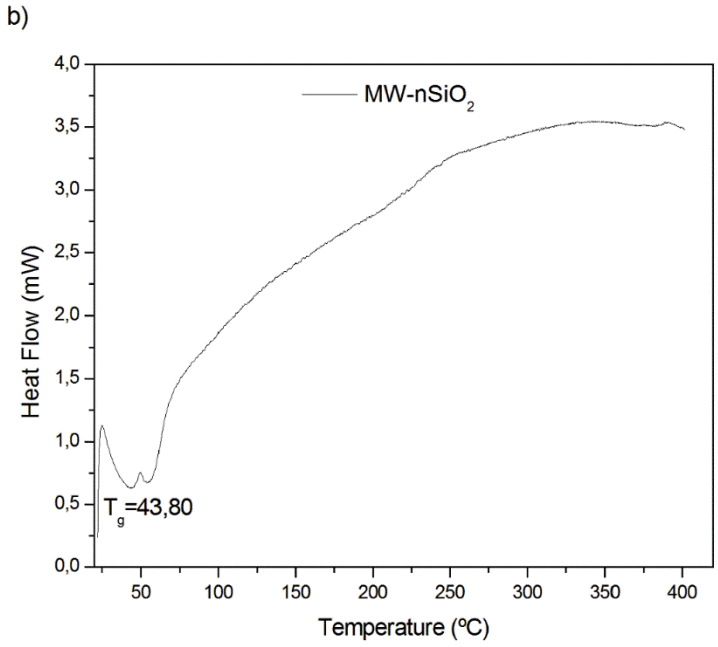

SEM images of $nSiO_2$ and MW–$nSiO_2$ are demonstrated in Fig. 26a and Fig. 26b. Fig. 26a shows that $nSiO_2$ generated from rice husk presented similar form in relation to the raw material (FERNANDES; SABINO; ROSSETTO, 2014). However, nanometric size was not attained using the standard process. In the sample MW–$nSiO_2$ (Fig. 26b), an agglomerate of spherical nanoparticles can be visualized, demonstrating that the microwave treatment was efficient in order to obtain SiO_2 in nanometric scale. The mean particle size of MW–$nSiO_2$ was estimated from the SEM images using the Image J software, and was 93±5 nm.

Figure 26 - SEM images of (a) $nSiO_2$ and (b) MW–$nSiO_2$.

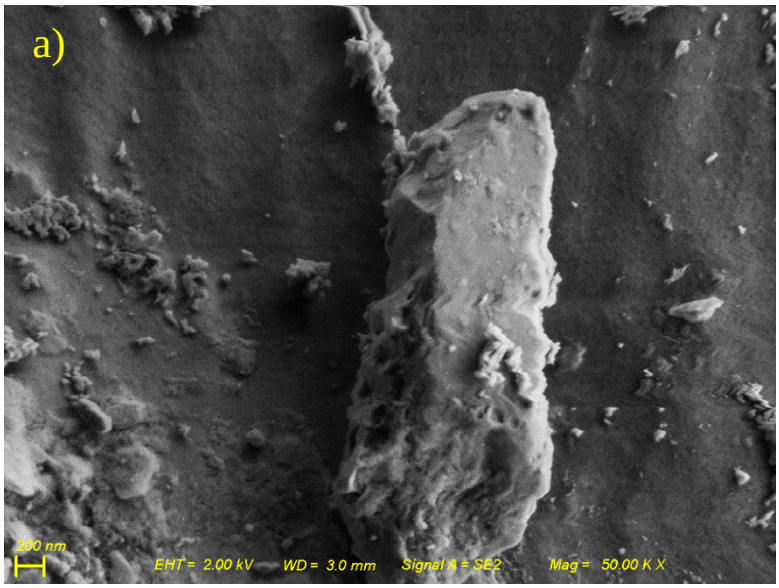

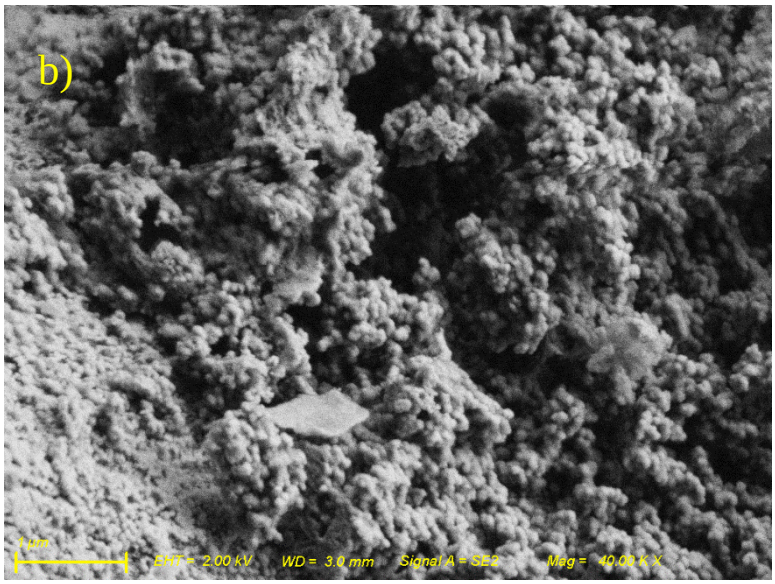

Based on the characterization techniques, it is possible affirm that the microwave synthesis presented advantages, in relation to the conventional process, to obtain silica nanoparticles from rice husk. The microwave route provided a material with better characteristics for dyes adsorption, like, higher values of surface area, pore volume, pore diameter and porosity. In addition, microwave leaching provided a material with higher purity in a shorter time (30 min). This occurred because, in comparison with traditional external heating methods, microwave heating is rapid volumetric heating without the heat conduction process, which can achieve uniform heating in a short period of time [29]. As consequence, the leaching is facilited.

5.3.2. Adsorbent dosage effect on Methylene Blue adsorption

The evaluation of adsorbent dosage is essential to determine the adequate amount of adsorbent to be utilized in order to attain major efficiency. In this work, the adsorbent dosage effect was evaluated using 100, 250, 500, 750 and 1000 mg L^{-1} of $nSiO_2$ and MW–$nSiO_2$. The results, in terms of dye removal percentage (%RE), are presented in Fig. 27. It can be seen that the adsorbent dosage increase caused an increase in MB removal percentage. This occurred due to the increase in the total amount of adsorption sites. For all adsorbent dosages, MW–$nSiO_2$ was superior in relation $nSiO_2$. The maximum %RE values were around 80 and 90% for $nSiO_2$ and

MW–$nSiO_2$, respectively. The better performance of MW–$nSiO_2$ to adsorb MB can be related with the more interesting characteristics of this material, like surface area, pore volume, pore diameter, porosity and purity, as presented in section 3.1. Based on these results, the adsorbent dosage of 1000 mg L^{-1} was selected for the subsequent tests.

Figure 27 - Adsorbent dosage effect on MB adsorption by (■) $nSiO_2$ and (●) MW–$nSiO_2$ (C_0=50 mg L^{-1}, 25 °C, 4 h).

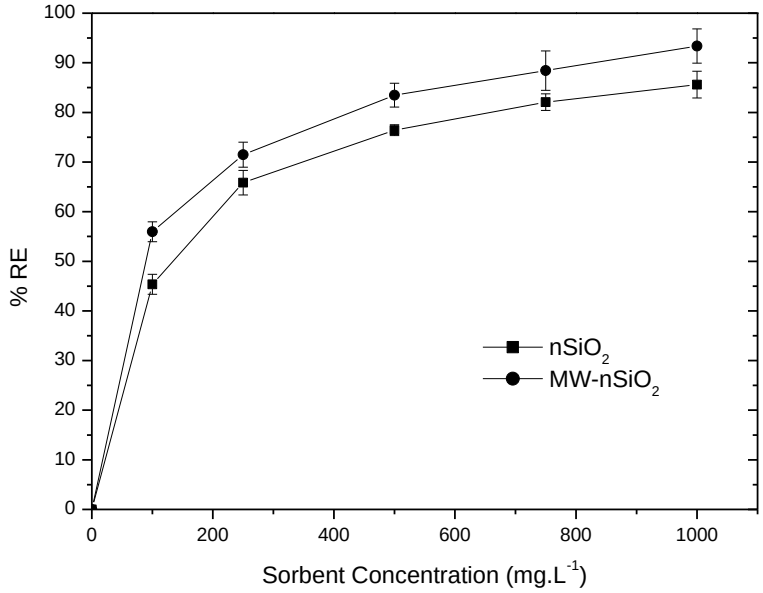

5.3.3. pH effect on Methylene Blue adsorption

pH is the most important factor in liquid phase adsorption, since affects the adsorbate chemistry in solution and also, the adsorbent surface. Here, pH effect was studied from 2 to 10, and the results are depicted in Fig. 28. For $nSiO_2$ and MW–$nSiO_2$, similar pH dependence was observed. The pH increase from 2 to 6 caused a strong increase in the adsorption capacity, but, a new increase, from 6 to 10 led to a decrease in adsorption capacity. To understand this pH dependence, the characteristics of MB and $nSiO_2$ based adsorbents should be take into account. The pKa of MB is equal to 5.6, so the MB molecule is cationic at pH higher than 5.6 and no ionic at pH lower than 5.6. The adsorbents contain Si–OH and O–Si–O groups (see section 3.1). Si–OH groups are

deprotonated above pH = 5 [30]. For O–Si–O groups, the point of zero charge is around 5 [31]. So, it can be inferred that, under acid conditions, the Si–OH and O–Si–O groups are neutral or protonated. So, MB molecules are repulsed or adsorbed by weak interactions. At pH 6, Si–OH and O–Si–O groups are deprotonated and MB is cationic, facilitating the interaction and increasing the adsorption capacity. However, under alkaline conditions, there is an excess of OH^- anions in solution and these are repulsed by the negatively charged surface of the adsorbents. As consequence, OH^- in solution compensates the MB positive charge, and this molecule become no ionic, hindering the interaction with the adsorbent surface and leading to a decrease in adsorption capacity. This result was similar to encountered by Hajjaji et al. [32], where the better adsorption capacity was found at pH 6.1, for a clay material containing silica in the composition. Based on these results, pH of 6.0 was selected to perform the subsequent studies.

Figure 28 - pH effect on MB adsorption by (●) $nSiO_2$ and (■) MW–$nSiO_2$ (C_0=50 mg L^{-1}, 25 °C, 4 h, adsorbent dosage of 1000 mg L^{-1}).

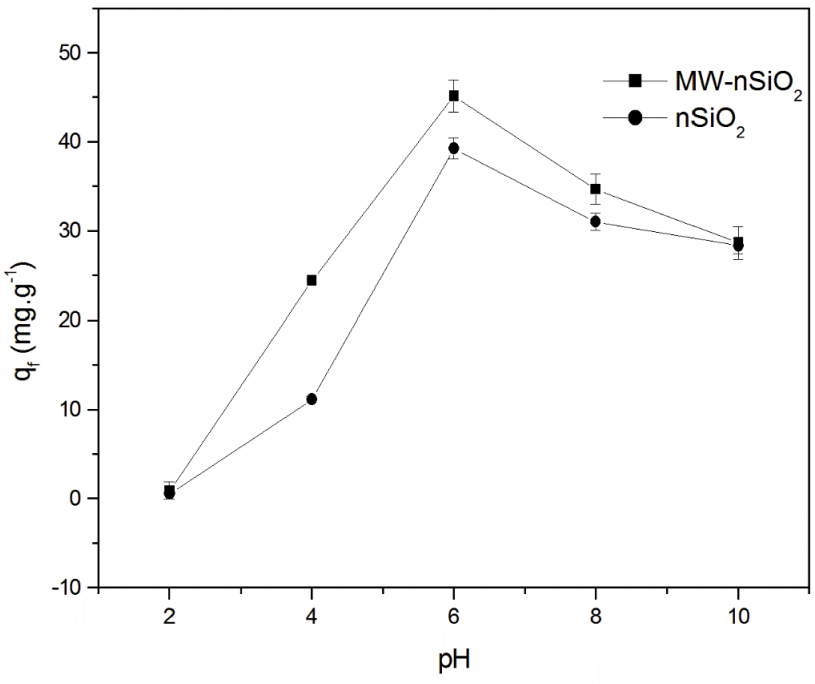

5.3.4. Kinetic studies

The kinetic curves were constructed with a range of contact time from 0 to 240 min, for initial MB concentrations of 50, 100, 200 and 300 mg L^{-1}, using adsorbent

dosage of 1000 mg L^{-1} at pH 6, for both adsorbents. Fig. 29 shows the kinetic curves for the MB adsorption onto $nSiO_2$ and MW–$nSiO_2$. For all conditions, typical kinetic curves were obtained, where, a fast step occurred until 5 min, and after, the adsorption rate was decreased, and finally, the curves tended to the equilibrium at 240 min. Evidently, higher values of adsorption capacity were found using higher initial dye concentrations.

Pseudo–first order (PFO), pseudo–second order (PSO) and pseudo–n order (PNO) models were investigated as reactions models to interpret the adsorption kinetic curves. The kinetic parameters for Methylene Blue adsorption on nSiO2 and MW–SiO2 are presented in Table 9. It was found that pseudo–n order model was the more adequate to represent the adsorption kinetics of MB on $nSiO_2$ and MW–$nSiO_2$, since presented higher values of coefficient of determination and lower values of AIC in relation to the other models (Table 9). In relation the parameters, q_n increased with the initial dye concentration, confirming that the adsorption capacity is favored at higher values of C_0. Moreover, q_n values for MW–$nSiO_2$ were higher than q_n values for $nSiO_2$, showing the efficiency of the microwave treatment in the adsorbent preparation.

Since PFO, PSO and PNO are reaction models, and consider adsorption as a reaction, in this work, a mass transfer based model (HSDM) was also utilized to interpret the kinetic curves. The experimental curves fitted with the HSDM model are presented in Fig. 30. The HSDM parameters are presented in Table 10. The high values of coefficient of determination the low values of AIC and ARE presented in Table 10 revealed that the HSDM model was adequate to represent the adsorption kinetics. The intraparticle diffusivity (D_{int}) values were higher for the microwave synthetized adsorbent (MW–$nSiO_2$) and increased with the initial dye concentration. This shows that the transference of MB molecules inside of MW–$nSiO_2$ is faster than the MB transference inside of $nSiO_2$ structure.

All kinetic studies revealed that MW–$nSiO_2$ is a better adsorbent for MB than $nSiO_2$, since presented higher values of adsorption capacities and faster adsorption rate. This result can be explained on the basis in the different characteristics of the materials. MW–$nSiO_2$ presented higher surface area, pore volume, pore diameter and porosity than $nSiO_2$, confirming the efficiency of microwave application. As consequence, the MB mass transfer on the internal structure of MW–$nSiO_2$ was facilitated (as demonstrated by the D_{int} values of HSDM model) and more adsorption sites were available, leading to higher adsorption capacities (as demonstrated by the q_n values of PNO model).

Figure 29 - Kinetic curves for Methylene Blue adsorption on (a) $nSiO_2$ and (b) $MW–nSiO_2$ (25 °C, pH of 6, adsorbent dosage of 1000 mg L^{-1}).

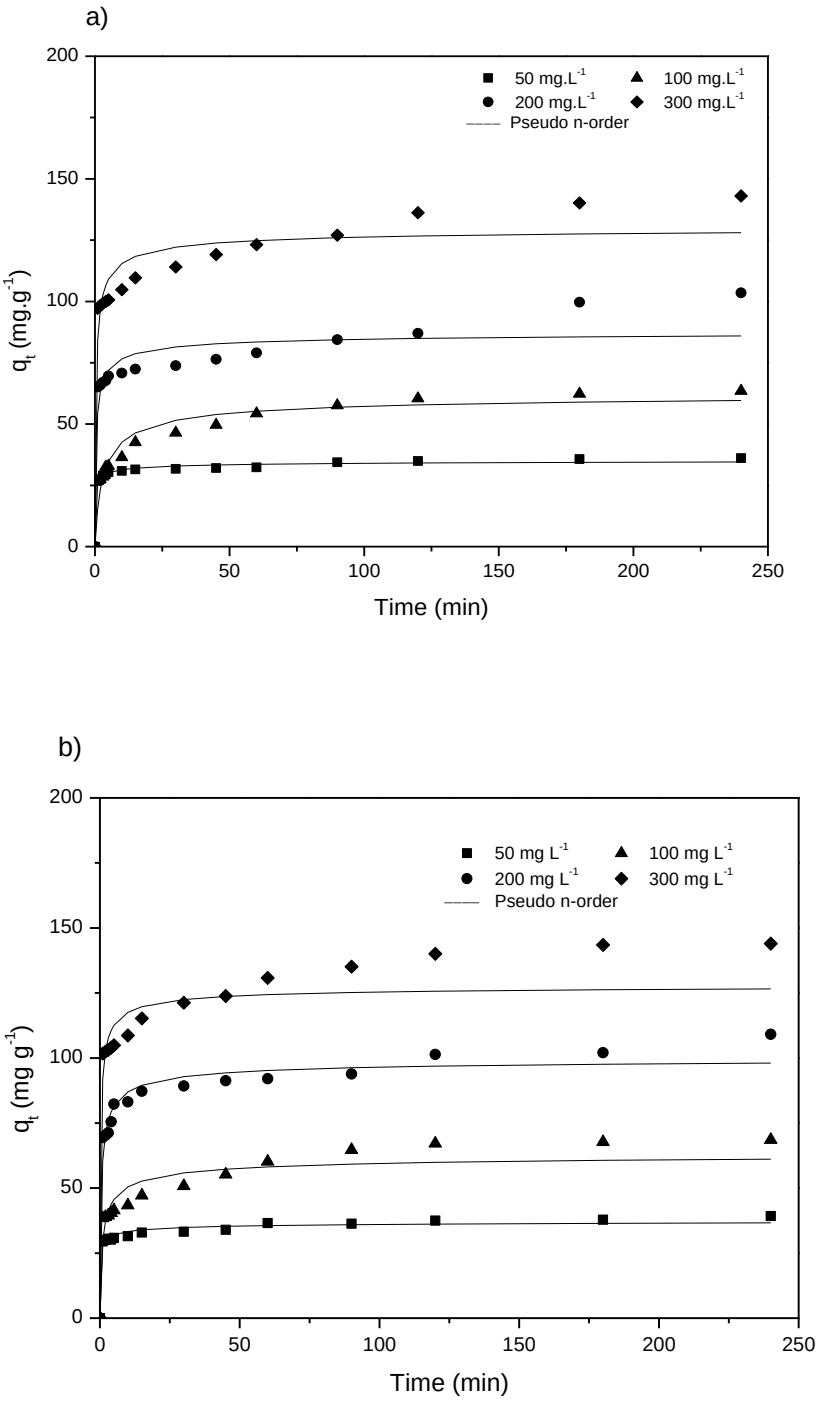

Table 9 - Kinetic parameters for the Methylene Blue adsorption on $nSiO_2$ and $MW–SiO_2$

Kinetic models	Dye concentration (mg L^{-1})							
	$nSiO_2$				$MW–nSiO_2$			
	50	100	200	300	50	100	200	300
PFO								
q_1 (mg g^{-1})	32.3	53.8	79.4	118.3	34.1	57.3	91.3	123.0
k_1 (min^{-1})	1.45	0.23	1.27	1.27	1.72	0.46	0.87	1.30
R^2	0.9649	0.8948	0.8808	0.9030	0.9489	0.8486	0.9241	0.9110
R^2_{adj}	0.9622	0.8867	0.8716	0.8955	0.9450	0.8369	0.9182	0.9042
ARE (%)	5.80	15.38	10.79	10.46	7.25	16.02	8.88	10.18
AIC	28.5	65.5	75.8	84.1	36.0	70.9	72.2	83.8
PSO								
q_2 (mg g^{-1})	33.4	57.6	83.6	124.8	35.4	60.8	95.5	129.7
k_2(g mg min^{-1})	0.0838	0.0057	0.0221	0.0145	0.0826	0.0115	0.0157	0.0143
R^2	0.9848	0.9490	0.9204	0.9455	0.9720	0.9190	0.9658	0.9531
R^2_{adj}	0.9836	0.9450	0.9142	0.9413	0.9698	0.9128	0.9631	0.9495
ARE (%)	4.07	10.63	8.61	7.65	5.48	11.74	5.98	7.34
AIC	16.1	55.1	70.1	75.8	27.2	70.9	60.6	83.8
PNO								
q_n (mg g^{-1})	36.1	63.3	88.4	129.2	38.9	64.7	101.0	131.5
k_n ((min^{-1}(g mg^{-1})$^{n-1}$)	0.0004	0.0002	0.0003	0.0002	0.0003	0.0001	0.0002	0.0007
n	3.93	2.78	3.05	2.97	3.99	3.27	3.01	2.83
R^2	0.9946	0.9658	0.9424	0.9659	0.9885	0.9510	0.9811	0.9617
R^2_{adj}	0.9937	0.9601	0.9329	0.9602	0.9865	0.9428	0.9779	0.9553
ARE (%)	2.19	8.72	6.86	6.11	3.45	9.04	4.42	1.86
AIC	3.8	52.4	68.6	68.6	17.2	57.9	55.0	74.7

Figure 30 - HSDM curves for Methylene Blue adsorption on (a) $nSiO_2$ and (b) $MW–nSiO_2$ (25 °C, pH of 6, adsorbent dosage of 1000 mg L^{-1}).

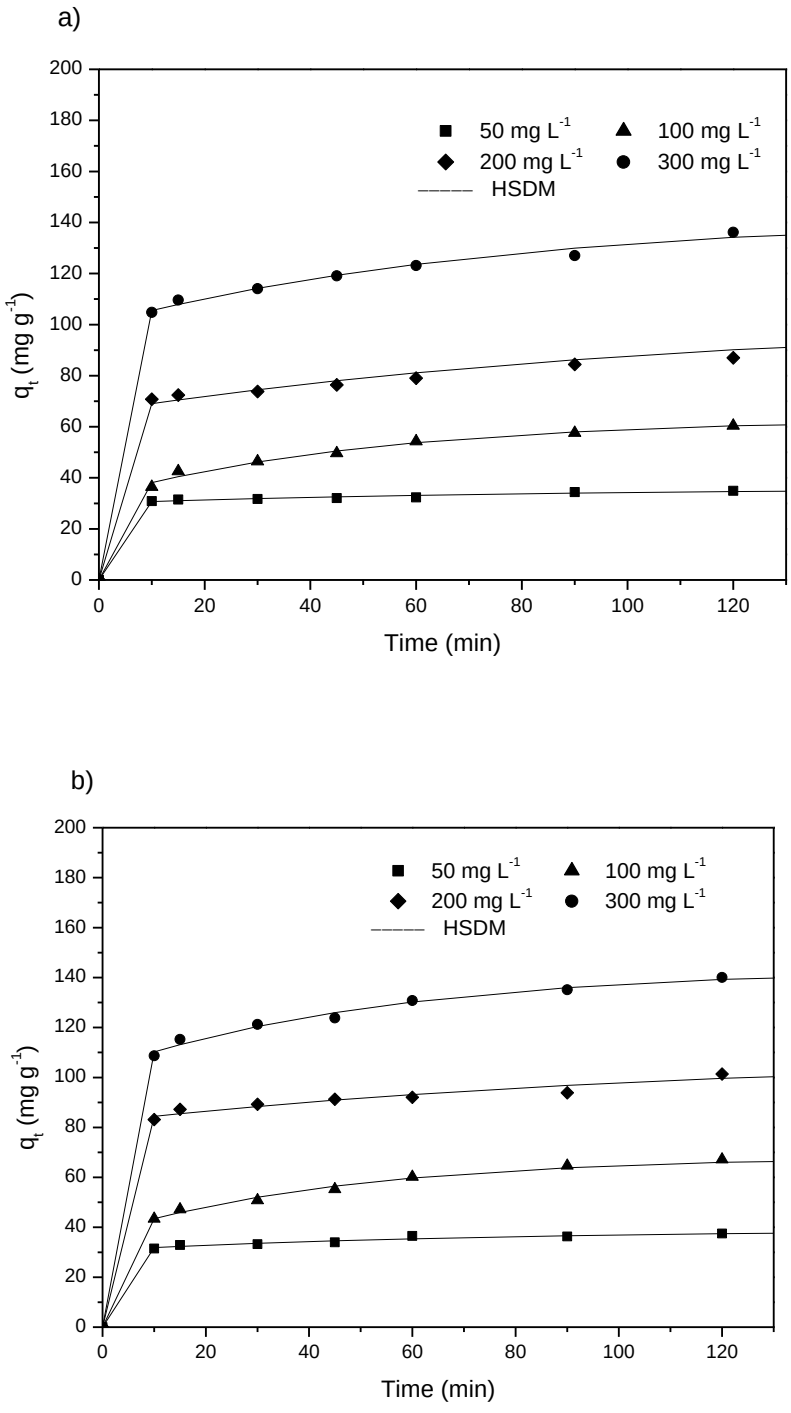

Table 10 - HSDM parameters for the Methylene Blue adsorption on $nSiO_2$ and $MW–SiO_2$.

HSDM model	Dye concentration (mg L^{-1})							
	$nSiO_2$				$MW–nSiO_2$			
	50	100	200	300	50	100	200	300
$D_{int} \times 10^{13}$ ($cm^2\ s^{-1}$)	1.92	4.39	1.70	2.42	2.18	4.60	1.81	2.45
R^2	0.9881	0.9876	0.9702	0.9859	0.9785	0.9909	0.9715	0.9815
ARE (%)	1.03	1.45	2.54	0.88	1.22	0.76	1.03	0.56
AIC	–12.42	4.43	24.74	13.07	–6.80	1.64	17.30	12.01

5.3.5. Equilibrium results

Equilibrium isotherms for MB adsorption on $nSiO_2$ and $MW–nSiO_2$ are presented in Figures 31a and 31b, respectively. All curves can be classified as 'L' curves (Langmuir Type). There is an initial curved portion at lower equilibrium concentrations, indicating the affinity adsorbate–adsorbent. The plateau was not attained in this concentration range, indicating that the adsorbents contain empty sites. Furthermore, it can be seen that the adsorption capacity was favored by the temperature decrease, being the higher values attained at 298 K.

Based on the shape of the isotherm curves, Langmuir, Freundlich and Sips models were selected to represent the MB adsorption on both adsorbents, and the results are presented in Table 11. For $nSiO_2$ and $MW–nSiO_2$, the Sips model presented higher values of coefficient of determination (R^2>0.99) and adjusted determination coefficient (R^2_{adj}>0.99), and lower values of Akaike information criterion (AIC) and average relative error (ARE) compared to the others models. In addition, the Sips parameters presented a clear trend in relation to the temperature. In this sense the Sips model was selected to represent the adsorption isotherms. The parameter k_S decreased with the temperature increase, indicating that the adsorption was disfavored at 328 K, and was better at 298 K. The q_s parameter increased with the temperature decrease, for both adsorbents, indicating that the adsorption capacity was favored at 298 K. Comparing now k_S and q_S between the adsorbents, it can be seen that $MW–nSiO_2$ presented the higher values of these parameters. This can be ascribed to the better characteristics of this material as adsorbent (see section 3.1).

MW–$nSiO_2$ attained maximum adsorption capacity of 679.9 mg g^{-1}. Liu et al. (LIU et al., 2012) obtained maximum adsorption capacity of 153.85 mg g^{-1} for MB, using graphene as adsorbent. Rida et al. (RIDA; BOURAOUI; HADNINE, 2013) studied the adsorption of Methylene Blue on kaolin and zeolite 4A, and found adsorption capacities of 45 and 22 mg g^{-1}, respectively. Polydopamine (PDA) microspheres were prepared by Fu et al. (FU et al., 2014) and employed for the adsorption of MB dye. The process variables were optimized and the maximum dye adsorption was 90.7 mg g^{-1}. Franco et al. [36] studied the MB adsorption on modified rice husk and found adsorption capacity of 65 mg g^{-1}. Based on these results it is possible affirm that MW–$nSiO_2$ is a suitable candidate to adsorb MB.

MW–$nSiO_2$ prepared in this work is an excellent adsorbent to remove MB from aqueous solutions. MW–$nSiO_2$ presents the main characteristics of silica, like thermal, mechanical and chemical resistance, coupled with fast adsorption kinetics, high adsorption capacity and high dye removal percentage. Furthermore, it was possible prove that the microwave treatment is adequate to obtain nanosilica with better characteristics for adsorption purposes.

Table 11 - Isotherm parameters for the Methylene Blue adsorption on nSiO2 and MW–$nSiO_2$.

Equilibrium Models	Temperature (K)							
	$nSiO_2$				MW–nSiO2			
	298	308	318	328	298	308	318	328
Langmuir								
q_m (mg g^{-1})	250.2	217.2	343.9	186.1	239.4	238.7	286.3	342.6
k_L (L mg^{-1})	0.009	0.008	0.002	0.004	0.011	0.009	0.005	0.003
R_L	0.695	0.710	0.891	0.830	0.643	0.683	0.815	0.888
R^2	0.9938	0.9865	0.9992	0.9985	0.9918	0.9932	0.9952	0.9967
R^2_{adj}	0.9923	0.9832	0.9991	0.9982	0.9898	0.9915	0.9940	0.9959
ARE (%)	8.50	12.06	3.47	4.81	10.08	8.39	5.95	5.72
AIC	31.44	34.35	16.76	17.11	33.30	31.66	29.07	25.88
Freundlich								
k_F (mg g^{-1})(mg L^{-})$^{-1/nf}$	11.02	9.446	2.386	3.253	14.12	11.47	5.130	2.459
$1/n_F$	0.496	0.493	0.720	0.602	0.457	0.483	0.609	0.717
R^2	0.9978	0.9984	0.9965	0.9901	0.9989	0.9967	0.9869	0.9914
R^2_{adj}	0.9972	0.9980	0.9956	0.9876	0.9987	0.9959	0.9836	0.9892
ARE (%)	4.80	3.11	8.78	11.98	2.35	5.12	11.22	11.04
AIC	25.33	21.64	25.99	28.55	21.11	27.28	35.05	31.60
Sips								
q_{mS} (mg g^{-1})	547.5	508.0	275.7	147.8	679.9	469.7	226.2	231.9
k_S(L mg^{-1})	0.014	0.002	0.002	0.002	0.016	0.016	0.002	0.001
m_S	0.635	0.503	1.122	1.251	0.557	0.644	1.262	1.297
R^2	0.9985	0.9983	0.9994	0.9999	0.9994	0.9978	0.9966	0.9987
R^2_{adj}	0.9976	0.9972	0.9991	0.9999	0.9990	0.9963	0.9943	0.9978
ARE (%)	3.31	3.05	1.75	0.39	1.44	3.40	7.88	5.30
AIC	32.82	31.86	25.99	9.18	27.83	34.92	37.04	30.47

Figure 31 - Equilibrium curves for Methylene Blue adsorption on (a) $nSiO_2$ and (b) $MW–nSiO_2$ (pH of 6, adsorbent dosage of 1000 mg L^{-1}).

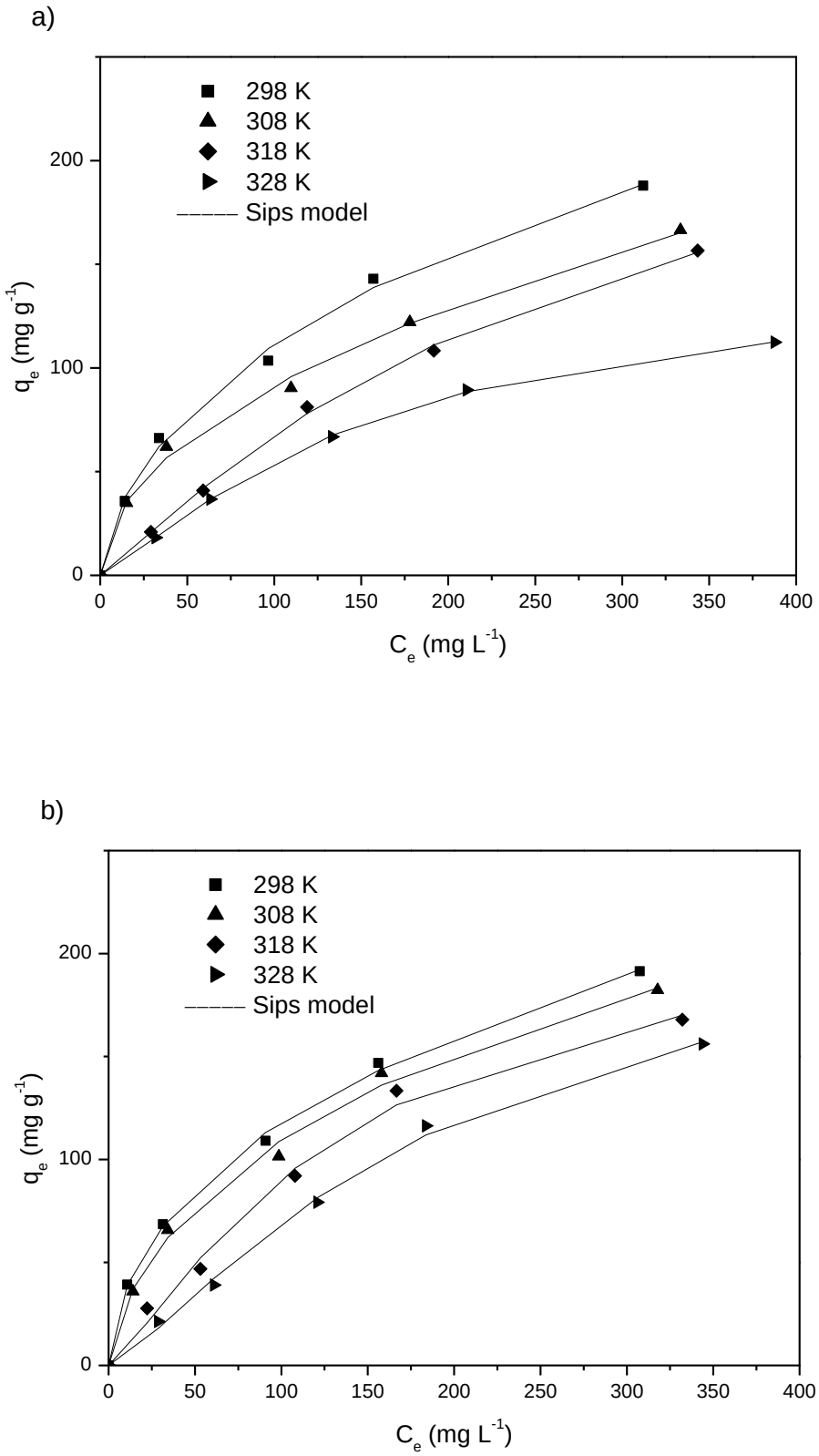

5.3.6. Thermodynamics results

Thermodynamic parameters (ΔG^0, ΔH^0 and ΔS^0) were estimated for both adsorbents, and are presented in Table 12. The values of standard thermodynamic constant (K) were estimated from the Sips parameters (K_s and q_s), because this model presented the best fit with the experimental data.

In relation to the Gibbs free energy change, favorable and spontaneous adsorption processes were verified for both adsorbents, since the values were negative. More negative ΔG^0 values were found at 298 K, indicating that adsorption was more favorable at lower temperatures. MB adsorption on $nSiO_2$ and MW–$nSiO_2$ were exothermic processes, since the ΔH^0 values were negative. ΔH^0 value for MB adsorption on MW–$nSiO_2$ was higher in relation to MB adsorption on $nSiO_2$. This indicates that the interactions MB/MW–$nSiO_2$ were relatively stronger. Based on the ΔH^0 magnitude, it is possible infer about the adsorption mechanism. Physisorption, such as van der Waals interactions, are usually lower than 20 kJ mol^{-1}, and electrostatic interaction ranges from 20 to 80 kJ mol^{-1}, chemisorption bond strengths can be from 80 to 450 kJ mol^{-1} (TRAN et al., 2017). Then, it is possible infer that chemical bonds occurred between MW–$nSiO_2$ and MB. Ionic chemical bonds between silica based materials and MB were recently reported by Saini et al. [13]. The positive ΔS^0 indicates the increase in the solid–liquid interface disorder demonstrating chemical affinity during the sorption process.

Table 12 - Thermodynamic parameters for the Methylene Blue adsorption on $nSiO_2$ and MW–$nSiO_2$.

Adsorbent	T (K)	ΔG^0 (kJ.mol^{-1})	ΔH^0 (kJ.mol^{-1})	ΔS^0 (kJ.mol^{-1}.K^{-1})
$nSiO_2$	298	–22.11	–86.6	0.2187
	308	–17.47		
	318	–16.47		
	328	–15.26		
MW–$nSiO_2$	298	–23.06	–115.1	0.3045
	308	–22.79		
	318	–16.14		
	328	–15.03		

5.4. CONCLUSION

In this research, silica nanoparticles were synthetized from rice husk by the microwave technology, aiming to improve the material characteristics and its potential to remove Methylene Blue from aqueous solutions. The characterization techniques like XRD, FT–IR, N_2 adsorption isotherms (BET and BJH), gas picnometry, DSC and SEM revealed that the microwave modified nano–silica (MW–$nSiO_2$) presented more interesting characteristics than the standard nano–silica ($nSiO_2$). Both materials were amorphous and presented typical FT–IR bands of silica. However, MW–$nSiO_2$ presented higher values of surface area, pore volume, pore diameter, porosity and purity than $nSiO_2$. Microwave technology was able to produce high purity nanosilica (98.8%) with particle size of 93 nm.

The Methylene Blue adsorption using $nSiO_2$ and MW–$nSiO_2$ was favored with adsorbent dosage of 1000 mg L^{-1} and pH of 6. The kinetic curves were adequately represented by pseudo–n order HSDM models. Sips equilibrium model was able to fit the MB adsorption on $nSiO_2$ and MB–$nSiO_2$. The maximum MB adsorption capacities were 547.5 mg g^{-1} and 679.9 mg g^{-1}, using $nSiO_2$ and MW–$nSiO_2$, respectively. Adsorption was spontaneous favorable and exothermic. The high ΔH^0 values (ΔH^0>80 kJ mol^{-1}) indicated that chemical bonds were involved in the dye/adsorbent interactions. It can be stated that MW–$nSiO_2$ prepared by the alternative microwave process, is an excellent adsorbent to remove MB from aqueous media, since presents the intrinsic characteristics of silica, like thermal, mechanical and chemical resistance, coupled with fast adsorption kinetics, high adsorption capacity and high dye removal percentage.

ACKNOWLEDGEMENTS

The authors would like to thank CAPES (Brazilian Agency for Improvement of Graduate Personnel), CNPq (National Council of Science and Technological Development) and FAPERGS for the financial support.

6. DISCUSSÃO DOS RESULTADOS

Os resultados obtidos neste trabalho propiciaram a elaboração de dois artigos de pesquisa que serão/estão publicados em periódicos da área de Engenharias II. Com o objetivo de avaliar a produção de nanosílica da casca de arroz utilizando rotas diferentes para lixiviação, resultados interessantes foram alcançados, os quais estão discutidos de forma global a seguir.

Em ambos os artigos foram produzidas o mesmo tipo de nano sílica padrão ($nSiO_2$) baseado no artigo de Sankar et al., 2016, utilizado como padrão para comparação com os processos de lixiviação com ultrassom (UM-$nSiO_2$) e micro-ondas (MW-$nSiO_2$), estas utilizadas para o primeiro e segundo trabalho, respectivamente.

No primeiro artigo foram avaliadas as características da $nSiO_2$ comparada a US-$nSiO_2$, analisando os principais parâmetros de caracterização como XRD, FTIR, DSC, MEV, BET, picnometria gasosa e XRF. Além disto, foram realizados os testes de adsorção para o corante Cristal Violeta (CV). Após, foram analisados os efeitos da dosagem de adsorvente, efeito do pH, curvas cinéticas, isotermas e estudo termodinâmico. Foram avaliados os modelos de Pseudo-Primeira Ordem (PFO) e Pseudo-Segunda Ordem (PSO), onde o melhor ajuste foi para o segundo modelo. Para representar as curvas de equilíbrio, BET e Freundlich foram os mais adequados, para a $nSiO_2$ e para UM-$nSiO_2$. Os melhores resultados foram obtidos para a UM-$nSiO_2$, que atingiu uma capacidade de adsorção de 495 mg g^{-1}, juntamente com a porcentagem de remoção de 98%, sendo um excelente adsorvente para o Cristal Violeta. Para ambos adsorventes, os resultados termodinâmicos revelaram um processo favorável, espontâneo e endotérmico.

No segundo artigo foram avaliadas a caracterização da $nSiO_2$ comparada a MW-$nSiO_2$, foram realizadas as mesmas análises presentes no primeiro artigo. O corante utilizado para os testes de adsorção do segundo artigo foi o azul de metileno (MB). Foram analisados as mesmas variáveis (dosagem de adsorvente, pH, tempo de contato e temperatura) do artigo anterior. Foram avaliados os modelos de Pseudo-Primeira Ordem (PFO) e Pseudo-Segunda Ordem (PSO), Pseudo-n Ordem e HSDM, onde o melhor ajuste ocorreu para o de Pseudo-n Ordem, sendo que o modelo HSDM foi avaliado separadamente para encontrar a difusividade do sistema de adsorção. Para representar as curvas de equilíbrio foram ajustados os modelos de Langmuir, Freundlich e Sips, onde o

modelo Sips foi o mais adequado. MW-nSiO_2 atingiu capacidade de adsorção de 679,9 mg g^{-1}, juntamente com porcentagem de remoção de 80%, sendo excelente adsorvente para corante MB, superior ao nSiO_2. Para ambos os adsorventes, os resultados termodinâmicos revelaram um processo favorável, espontâneo e exotérmico.

Comparando os resultados de caracterização juntamente, nota-se que de acordo com o XRD, que todas as amostras demostraram estruturas amorfas, em ambos os artigos, sendo que não houve diferença entre essas estruturas. De acordo com artigos citados anteriormente, a organização da estrutura da sílica produzida ocorre a partir de 700°C na etapa de queima da casca de arroz. Outra análise, que não demonstrou diferença entre as nano-partículas de sílica produzidas foi o FTIR, pois apenas a forma de transferência de massa e calor mudava, e não os grupos funcionais presentes na estrutura. Sendo assim as bandas apresentadas comparando os três tipos de nano sílica produzidas são idênticas.

Em relação ás imagens de microscopia eletrônica de varredura (MEV), foram utilizadas para a determinação do tamanho da partícula e para a comprovação que o material utilizado nesta dissertação tem o tamanho de nanopartículas em todos os cenários em que foi produzida. Já em relação ao XRF, este foi utilizado para determinação da pureza produzida, onde a nano sílica com maior pureza foi a produzida através do ultrassom com cerca de 99,5% de sílica presente. Comparando os processos de lixiviação, o ultrassom é o processo mais rápido (lixiviação em cerca de 10 minutos), e com maior efetividade na remoção de outras impurezas presentes na casca. A retirada destes elementos (outros sais metálicos presentes na casca) pode ser um dos motivos para a maior porosidade do UM-nSiO_2

Outro resultado considerado importante diz respeito a quantidade é o resultado da análise do BET, estudada conjuntamente com a picnometria gasosa para a estimativa de outras propriedades como a porosidade do material. Em relação ao BET, a maior área superficial foi apresentada pela UM-nSiO_2 (91,05 $m^2\ g^{-1}$), seguida pelo tratamento de micro-ondas, MW-nSiO_2 (84,56 $m^2\ g^{-1}$), e por último a nSiO_2 produzida através do método padrão (71,97 $m^2\ g^{-1}$), isto demonstra que o processo de ultrassom gerou o material com maior capacidade para ser um bom adsorvente, comprovado também por outros parâmetros, como maior porosidade e maior volume de poros. Como os artigos foram comparados separadamente o processo por micro-ondas e por ultrassom, não é possível estimar, o quanto a UM-nSiO_2 é superior a MW-nSiO_2, para a adsorção de azul de metileno. Devido aos valores apresentados de área superficial, volume de poros,

diâmetro médio de poros e porosidade, e como não há diferença entre as análises de FTIR, é possível acreditar que os resultados de adsorção para a MW-nSiO_2 teriam valores superiores a nSiO_2 e inferiores a UM-nSiO_2. Todos os materiais apresentaram similaridade quanto o tipo de poros, sendo materiais mesoporosos.

Em relação ao DSC, todos materiais demonstraram o mesmo comportamento para a degradação de água, porém a nSiO_2, apresentou um pico em torno de 250 °C indicando a degradação de materiais residuais, que não foram removidos durante a preparação do processo convencional. Por outro lado, este pico não foi verificado para a MW-nSiO2 e UM-nSiO_2, indicando que o processo de micro-ondas e ultrassom foram mais eficientes para fornecer materiais de alta pureza.

Em relação aos testes de adsorção, a comparação entre adsorventes é imprópria para ser feita devido aos experimentos serem realizados para diferentes corantes (Cristal Violeta e Azul de Metileno). Verificou-se que o comportamento das isotermas foram diferentes para cada um dos corantes, sendo que para cada artigo foi necessário ajustar modelos em decorrência do diferente formato das curvas. No geral, é possível apenas que o adsorvente com maior potencial para novos experimentos é a UM-nSiO_2, devido aos resultados superiores em todas as análises de caracterização e a grande capacidade de adsorção apresentada para o corante Cristal Violeta. Para trabalhos futuros, poderiam ser realizados testes com outros corantes, para testar o potencial de adsorção e comparar a UM-nSiO_2 a MW-nSiO2.

7. CONCLUSÃO

A busca por alternativas para o tratamento de resíduos gerados da casca de arroz consolidou a queima como principal método de utilização deste material, gerando enorme quantidade cinzas para serem descartadas. Este trabalho visou a busca de uma alternativa para utilização e resolução de ouros problema ambiental, o tratamento de efluentes líquidos da indústria de corantes. A utilização de um resíduo sólido, sem custo como as cinzas, para tratamento de um resíduo líquido é de enorme contribuição na busca de alternativas sustentáveis, visando a proteção ambiental em relação ao descarte destes resíduos. Através de duas diferentes rotas de produção de nano sílica através das cinzas da casca de arroz, foram analisadas as melhorias realizadas nestes materiais para a utilização posterior no tratamento de dois diferentes tipos de corantes catiônicos.

Na primeira parte do trabalho, foram produzidas duas amostras de nano sílica: a primeira através da rota convencional ($nSiO_2$) e a segunda através de uma rota de lixiviação através de ultrassom (UM-$nSiO_2$). Ambos os materiais ($nSiO_2$ e UM-$nSiO_2$) foram amorfos e apresentaram grupos funcionais típicos de sílica. A nano sílica preparada através do ultrassom (UM-$nSiO_2$) apresentou área de superfície 30% maior do que o material preparado pelo processo convencional (nSiO2). Em relação ao volume de poros, o diâmetro dos poros, a densidade, a porosidade e a pureza também foram maiores para UM-$nSiO_2$. Os primeiros testes de adsorção realizados para o cristal violeta (CV) foram o efeito da massa e pH, onde os melhores resultados foram para de 1000 mg L^{-1} e pH de 10. As curvas cinéticas foram melhores ajustadas pelo modelo de Pseudo-segunda ordem. Em relação aos modelos de equilíbrio, BET foi mais adequado para a isoterma da $nSiO_2$, enquanto utilizando Freundlich obteve-se melhor ajuste da UM-$nSiO_2$. Em geral, a capacidade de adsorção da UM-$nSiO_2$ foi 15% maior em relação ao $nSiO_2$. UM-$nSiO_2$ atingiu capacidade de adsorção de 495 mg g^{-1}, juntamente com porcentagem de remoção de 98%. Em resumo, pode-se afirmar que UM-nSiO2 preparado pelo processo de ultrassom alternativo, é um excelente adsorvente para remover CV de meios aquosos, devido à alta capacidade de adsorção e alta porcentagem de remoção do corante.

Em relação á segunda parte do trabalho, foi produzida outra amostra de nano sílica através de uma rota de lixiviação através de micro-ondas (MW-$nSiO_2$), e os resultados foram comparados com a nano sílica ($nSiO_2$) do processo convencional

preparada anteriormente. Como o primeiro artigo, ambos os materiais foram amorfos e apresentaram as mesmas bandas de FT-IR, típicas de sílica. No entanto, MW-nSiO2 também apresentou maiores valores de área superficial, volume de poros, diâmetro dos poros, porosidade, mas destacando-se principalmente a pureza (98,8%) com tamanho de partícula de 93 nm em relação a $nSiO_2$. Os testes de dosagem de adsorvente e pH, resultaram nas condições de 1000 mg L^{-1} e pH de 6. Os modelos cinéticos que melhor se ajustaram foram o HSDM e de pseudo-n ordem. Para as isotermas, Sips foi o modelo para representação do equilíbrio, obtendo-se os melhores valores de AIC e R^2_{adj}. As capacidades máximas de adsorção de MB foram 547,5 mg g^{-1} e 679,9 mg g^{-1}, utilizando $nSiO_2$ e MW-$nSiO_2$, respectivamente. A adsorção foi espontânea favorável e exotérmica. Devido aos bons resultados para adsorção de azul de metileno, pode-se afirmar que o MW-$nSiO_2$ preparado pela lixiviação por micro-ondas é um adsorvente promissor, devido as características apresentadas como a adsorção rápida, alto valor da capacidade de adsorção e alta porcentagem de remoção de corantes.

REFERÊNCIAS BIBLIOGRÁFICAS

ABDEL-HALIEM, M. E. F. et al. Effect of silica ions and nano silica on rice plants under salinity stress. **Ecological Engineering**, v. 99, p. 282–289, 2017.

ABRAFATI. **Indicadores do mercado de tintas**. Disponível em: <https://www.abrafati.com.br/indicadores-do-mercado/numeros-do-setor/>. Acesso em: 23 nov. 2016.

AGGARWAL, P.; SINGH, R. P.; AGGARWAL, Y. Use of nano-silica in cement based materials—A review. **Cogent Engineering**, v. 2, n. 1, 2015.

AHMAD, R. Studies on adsorption of crystal violet dye from aqueous solution onto coniferous pinus bark powder (CPBP). **Journal of Hazardous Materials**, v. 171, p. 767–773, 2009.

AJMAL, M. et al. Adsorption studies on rice husk : removal and recovery of Cd (II) from wastewater. **Bioresource Technology**, v. 86, p. 147–149, 2003.

AL-OWEINI, R.; EL-RASSY, H. Synthesis and characterization by FTIR spectroscopy of silica aerogels prepared using several Si(OR)4 and R″Si(OR′)3 precursors. **Journal of Molecular Structure**, v. 919, n. 1–3, p. 140–145, 2009.

ALMEIDA, L. P. DE. **Caracterização de Pigmentos da Curcuma longa L., Avaliação da Atividade Antimicrobiana, Morfogênese in vitro na Produção de Curcuminóides e Óleos Essenciais**. [s.l.] UFMG, 2006.

AMMENDOLA, P.; RAGANATI, F.; CHIRONE, R. CO2 adsorption on a fine activated carbon in a sound assisted fluidized bed: Thermodynamics and kinetics. **Chemical Engineering Journal**, v. 322, p. 302–313, 2017.

BALABANOVA, E. Silica nanoparticles produced by thermal arc plasma. **Journal of Optoelectronics and Advanced Materials**, v. 5, n. 3, p. 679–686, 2003.

BELCHIOR, M.; TAI, D. W.; HELD, F. C. VON. **Indicadores IBGE**. Disponível em: <https://www.ibge.gov.br/estatisticas-novoportal/economicas/agricultura-e-pecuaria/9201-levantamento-sistematico-da-producao-agricola.html?&t=destaques>. Acesso em: 24 nov. 2017.

BIRICIK, H.; SARIER, N. Comparative study of the characteristics of nano silica - , silica fume - and fly ash - incorporated cement mortars. **Materials Research**, v. 17, n. 3, p. 570–582, 2014.

BREITBACH, M.; BATHEN, D.; SCHMIDT-TRAUB, H. Effect of Ultrasound on Adsorption and Desorption Processes. **Industrial & Engineering Chemistry Research**, v. 42, n. 22, p. 5635–5646, 2003.

BRIÃO, G. V. et al. Adsorption of Crystal Violet Dye onto a Mesoporous ZSM–5 Zeolite Synthetized using Chitin as Template. **Journal of Colloid and Interface Science**, v. 508, p. 313–322, 2017.

CHAKRABORTY, S. et al. Adsorption of Crystal Violet from aqueous solution onto. **Carbohydrate Polymers**, v. 86, n. 4, p. 1533–1541, 2011.

CHANDRASEKHAR, S. et al. Review Processing, properties and applications of reactive silica from rice husk—an overview. **Journal of Materials Science**, v. 38, n. 15, p. 3159–3168, 2003.

CHEN, L. et al. High performance agar/graphene oxide composite aerogel for methylene blue removal. **Carbohydrate Polymers**, v. 155, p. 345–353, 2017.

CHESHMEH, R. D. et al. International Biodeterioration & Biodegradation Preparation of bio-silica / chitosan nanocomposite for adsorption of a textile dye in aqueous solutions. **International Biodeterioration & Biodegradation**, v. 85, p. 383–391, 2013.

CHIOU, M. S.; HO, P. Y.; LI, H. Y. Adsorption of anionic dyes in acid solutions using chemically cross-linked chitosan beads. **Dyes and Pigments**, v. 60, n. 1, p. 69–84, 2004.

CRANK, J. **The mathematics of diffusion**. 1. ed. Oxford: Clarendon Press, 1979.

DĄBROWSKI, A. Adsorption - From theory to practice. **Advances in Colloid and Interface Science**, v. 93, n. 1–3, p. 135–224, 2001.

DAFFALLA, S. B.; MUKHTAR, H.; SHAHARUN, M. S. Caracterization of Absorbent Developed from Rice Husk: Effect of Surface Functional Group on Phenol Absorption. **Journal of Applied Sciences**, v. 10, n. DECEMBER, p. 1060–1067, 2010.

DOTTO, G. L. et al. Surface modification of chitin using ultrasound-assisted and

supercritical CO2 technologies for cobalt adsorption. **Journal of Hazardous Materials**, v. 295, p. 29–36, 2015.

DOTTO, G. L.; PINTO, L. A. A. Analysis of mass transfer kinetics in the biosorption of synthetic dyes onto Spirulina platensis nanoparticles. **Biochemical Engineering Journal**, v. 68, p. 85–90, 2012.

EBADI, A.; SOLTAN MOHAMMADZADEH, J. S.; KHUDIEV, A. What is the correct form of BET isotherm for modeling liquid phase adsorption? **Adsorption**, v. 15, n. 1, p. 65–73, 2009.

ERDEM, N.; AKŞIT, A.; H. ERDOGAN, U. Flame Retardancy Behaviors and Structural Properties of Polypropylene/Nano-SiO2 Composite Textile Filaments. **Journal of Applied Polymer Science**, v. 111, p. 2085–2091, 2009.

FANGLONG, Z. et al. Influence of nano-silica on flame resistance behavior of intumescent flame retardant cellulosic textiles: Remarkable synergistic effect? **Surface and Coatings Technology**, v. 294, p. 90–94, 2016.

FERNANDES, L.; SABINO, M. G.; ROSSETTO, H. L. Método de extração de sílica da casca do arroz. **Cerâmica**, v. 60, n. 353, p. 160–163, 2014.

FERREIRA, L. S. et al. Adsorption of Ni 2+, Zn 2+ and Pb 2+ onto dry biomass of Arthrospira (Spirulina) platensis and Chlorella vulgaris. I. Single metal systems. **Chemical Engineering Journal**, v. 173, n. 2, p. 326–333, 2011.

FOLETTO, E. L. et al. Applicability of Rice Husk Ash. **Química Nova**, v. 28, n. 6, p. 1055–1060, 2005.

FRANCO, D. S. P. et al. Adsorption of Co(II) from aqueous solutions onto rice husk modified by ultrasound assisted and supercritical technologies. **Process Safety and Environmental Protection**, v. 109, n. Ii, p. 55–62, 2017.

FREUNDLICH, H. Over the adsorption in solution. **Z. Physic. Chem**, n. A57, p. 358–471, 1906.

FU, J. et al. Adsorption of methylene blue by a high-efficiency adsorbent (polydopamine microspheres): Kinetics, isotherm, thermodynamics and mechanism analysis. **Chemical Engineering Journal**, 2014.

G. RITCHIE, A. Alternative to the Elovic Equation for the Kinetics of Adsorption of Gases on Solids. **J. Chem. Soc., Faraday Trans. 1**, v. 73, 1977.

GHORBANI, F.; SANATI, A. M.; MALEKI, M. Production of Silica Nanoparticles from Rice Husk as Agricultural Waste by Environmental Friendly Technique. **Environmental Studies of Persian Gulf**, v. 2, n. 1, p. 56–65, 2015.

GILES, C. H. et al. A System of Classication of Solution Adsorption Isotherms, and its Use in Diagnosis of Adsorption Mechanisms and in Measurement of Specific Surface Areas of Solids. **Studies in Adsorption XI**, v. 846, 1958.

GUARATINI, C. C. I.; ZANONI, V. B. Fixação do Corante A forma de fixação da molécula do corante a essas fibras geralmente é feita em solução aquosa e pode envolver basicamente. **Química Nova**, v. 23, n. 1, p. 71–78, 1999.

GUO, W. et al. Adsorption of perfluorooctane sulfonate (PFOS) on corn straw-derived biochar prepared at different pyrolytic temperatures. **Journal of the Taiwan Institute of Chemical Engineers**, v. 0, p. 1–7, 2017.

GUPTA, S. et al. Nanocarriers and nanoparticles for skin care and dermatological treatments. **Indian Dermatology Online Journal**, v. 4, n. 4, p. 267–272, 2013.

GUPTA, V. K.; SUHAS. Application of low-cost adsorbents for dye removal - A review. **Journal of Environmental Management**, v. 90, n. 8, p. 2313–2342, 2009.

HALLIDAY, D.; RESNICK, R.; WALKER, J. **Fundamentos de Física**. 8. ed. [s.l: s.n.].

HARO, N. K. et al. Removal of atenolol by adsorption – Study of kinetics and equilibrium. **Journal of Cleaner Production**, v. 154, p. 214–219, 2017.

HICKERT, L. R. **Otimização da hidrólise de casca de arroz (Oryza sativa) e avaliação da capacidade de bioconversão deste hidrolisado a etanol e xilitol por leveduras**. [s.l.] Universidade Federal do Rio Grande do Sul, 2010.

HO, Y. S. et al. Sorption of lead ions from aqueous solution using tree fern as a sorbent. **Hydrometallurgy**, v. 73, n. 1–2, p. 55–61, 2004.

HO, Y. S.; MCKAY, G. Pseudo-second order model for sorption processes. **Process Biochemistry**, v. 34, n. 5, p. 451–465, 1999.

INGLEZAKIS, V.; POULOPOULOS, S. G. **Adsorption, Ion Exchange and Catalysis: Design of Operations and Environmental Application**. 1. ed. [s.l.] Elsevier, 2006.

JI-LU, Z. Bio-oil from fast pyrolysis of rice husk: Yields and related properties and improvement of the pyrolysis system. **Journal of Analytical and Applied Pyrolysis**, v. 80, n. 1, p. 30–35, 2007.

KAMAT, P. V. Quantum Dot Solar Cells. Semiconductor Nanocrystals as Light Harvesters†. **J. Phys. Chem. C**, v. 112, n. 48, p. 18737–18753, 2008.

KAPPE, C. O.; DALLINGER, D. Controlled microwave heating in modern organic synthesis: Highlights from the 2004-2008 literature. **Molecular Diversity**, v. 13, n. 2, p. 71–193, 2009.

KULKARNI, M. R. et al. Removal of Crystal Violet dye from aqueous solution using water hyacinth : Equilibrium , kinetics and thermodynamics study. **Resource-Efficient Technologies**, v. 3, n. 1, p. 71–77, 2017.

LAGERGREN, S. About the theory of so–called adsorption of soluble substances. **Kungliga Svenska Vetenskapsakademiens**, v. 24, p. 1–39, 1898.

LANGMUIR, I. The adsorption of gases on plane surfaces of glass, mica and platinum. **The Journal of the American Chemical Society**, v. 40, n. 9, p. 1361–1403, 1918a.

LANGMUIR, I. The adsorption of gases on plane surfaces of glass. **Journal of the American Chemical Society**, v. 345, n. 1914, 1918b.

LARHED, M.; OLOFSSON, K. **Microwave methods in organic synthesis**. 1. ed. Berlin: Springer, 2006.

LAZARO, A. et al. The properties of amorphous nano-silica synthesized by the dissolution of olivine. **Chemical Engineering Journal**, v. 211–212, n. 2012, p. 112–121, 2012.

LAZARO, A. et al. Synthesis of a Green Nano-Silica Material Using Beneficiated Waste Dunites and Its Application in Concrete. **World Journal of Nano Science and Engineering**, v. 3, n. 3, p. 41–51, 2013.

LAZARO, A.; QUERCIA, G.; BROUWERS, H. J. H. Production and application of a

new type of nano-silica in concrete. **International Congress on Durability of Concrete**, v. 2, p. 466–473, 2012.

LEÃO, M. M. D. **Controle ambiental na indústria têxtil: acabamento de malhas**. [s.l.] SEGRAC - Editora e Gráfica, 2002.

LIDSTRÖM, P. et al. Microwave assisted organic synthesis—a review. **Tetrahedron**, v. 57, n. 45, p. 9225–9283, 2001.

LIOU, T. H. Preparation and characterization of nano-structured silica from rice husk. **Materials Science and Engineering A**, v. 364, n. 1–2, p. 313–323, 2004.

LIU, T. et al. Colloids and Surfaces B : Biointerfaces Adsorption of methylene blue from aqueous solution by graphene. **Colloids and Surfaces B: Biointerfaces**, v. 90, p. 197–203, 2012.

MA'RUF, A.; PRAMUDONO, B.; ARYANTI, N. Lignin isolation process from rice husk by alkaline hydrogen peroxide: Lignin and silica extracted. **AIP Conference Proceedings**, v. 1823, 2017.

MA, F.; ZHAO, B.; DIAO, J. Adsorption of cadmium by biochar produced from pyrolysis of corn stalk in aqueous solution. **Water Science and Technology**, v. 74, n. 6, p. 1335–1345, 2016.

MALIK, P. K. Use of activated carbons prepared from sawdust and rice-husk for adsoprtion of acid dyes: A case study of acid yellow 36. **Dyes and Pigments**, v. 56, n. 3, p. 239–249, 2003.

MALIK, R.; RAMTEKE, D. S.; WATE, S. R. Adsorption of malachite green on groundnut shell waste based powdered activated carbon. **Waste Management**, v. 27, n. 9, p. 1129–1138, 2007.

MAYER, F. D.; HOFFMANN, R.; RUPPENTHAL, J. E. Gestão Energética , Econômica e Ambiental do Resíduo Casca de Arroz em Pequenas e Médias Agroindústrias de Arroz. **Xiii Simpep**, p. 1–11, 2006.

MESTANZA, S. N. M. et al. Study of the influence of dynamics variables on the growth of silica nanoparticles. **Inorganic and Nano-Metal Chemistry**, v. 47, n. 6, p. 824–829, 2017.

MUSIĆ, S.; FILIPOVIĆ-VINCEKOVIĆ, N.; SEKOVANIĆ, L. Precipitation of amorphous SiO2 particules and their properties. **Brazilian Journal of Chemical Engineering**, v. 28, n. 1, p. 89–94, 2011.

PARAB, H. et al. Determination of kinetic and equilibrium parameters of the batch adsorption of Co(II), Cr(III) and Ni(II) onto coir pith. **Process Biochemistry**, v. 41, n. 3, p. 609–615, 2006.

PATEL, M.; KARERA, A.; PRASANNA, P. Effect of thermal and chemical treatments on carbon and silica contents in rice husk. **Journal of Materials Science**, v. 22, n. 7, p. 2457–2464, 1987.

PENG, Q. et al. Adsorption of dyes in aqueous solutions by chitosan – halloysite nanotubes composite hydrogel beads. **Microporous and Mesoporous Materials**, v. 201, p. 190–201, 2015.

PETERS, T. M. et al. Airborne monitoring to distinguish engineered nanomaterials from incidental particles for environmental health and safety. **Journal of Occupational and Environmental Hygiene**, v. 6, n. 2, p. 73–81, 2009.

POTAPOV, V. V et al. Silica Powders Production from Hydrothermal Solutions. **Workshop on Geothermal Reservoir Engineering**, v. 36, 2011.

QIU, H. et al. Critical review in adsorption kinetic models. **Journal of Zhejiang University- Science A**, v. 10, n. 5, p. 716–724, 2009.

RIDA, K.; BOURAOUI, S.; HADNINE, S. Applied Clay Science Adsorption of methylene blue from aqueous solution by kaolin and zeolite. **Applied Clay Science**, v. 83–84, p. 99–105, 2013.

ROSA, M. P. et al. Extraction of Organosolv Lignin From Rice Husk Under Reflux Conditions. **Biological and Chemical Research**, p. 87–98, 2016.

RUDZINSKI, W.; PLAZINSKI, W. Theoretical description of the kinetics of solute adsorption at heterogeneous solid/solution interfaces. **Applied Surface Science**, v. 253, n. 13, p. 5827–5840, 2007.

RUTHVEN, D. M. **Principles of adsorption and adsorption processes**New YorkWiley-Interscience, , 1984.

SALLEH, M. A. M. et al. Cationic and anionic dye adsorption by agricultural solid wastes: A comprehensive review. **Desalination**, v. 280, n. 1–3, p. 1–13, 2011.

SANKAR, S. et al. Biogenerated silica nanoparticles synthesized from sticky, red, and brown rice husk ashes by a chemical method. **Ceramics International**, v. 42, n. 4, p. 4875–4885, 2016.

SARANGI, M.; BHATTACHARYYA, S.; BEHERA, R. C. Effect of temperature on morphology and phase transformations of nano-crystalline silica obtained from rice husk. **Phase Transitions**, v. 82, n. 5, p. 377–386, 2009.

SARKER, N.; FAKHRUDDIN, A. N. . Removal of phenol from aqueous solution using rice straw as adsorbent. **Applied Water Science**, 2015.

SENTHILKUMAAR, S.; KALAAMANI, P.; SUBBURAAM, C. V. Liquid phase adsorption of Crystal violet onto activated carbons derived from male flowers of coconut tree. **Journal of Hazardous Materials**, v. 136, n. 3, p. 800–808, 2006.

SEOW, T. W.; LIM, C. K. Removal of dye by adsorption: A review. **International Journal of Applied Engineering Research**, v. 11, n. 4, p. 2675–2679, 2016.

SHOUKAT, S. et al. Mango stone biocomposite preparation and application for crystal violet adsorption: A mechanistic study. **Microporous and Mesoporous Materials**, v. 239, p. 180–189, 2016.

SINGH, D. et al. Synthesis and characterization of rice husk silica , silica-carbon composite and H - 3 PO 4 activated silica. **Cerâmica**, v. 54, p. 203–212, 2008.

SINGH, V. et al. Ultrasound: A boon in the synthesis of organic compounds. **Resonance**, v. 3, n. 9, p. 56–60, 1998.

SIPS, R. The Structure of a Catalyst Surface. **The Journal of Chemical Physics**, v. 16, p. 490–495, 1948.

SODIPO, B. K.; AZIZ, A. A. One minute synthesis of amino-silane functionalized superparamagnetic iron oxide nanoparticles by sonochemical method. **Ultrasonics Sonochemistry**, v. 40, n. August 2017, p. 837–840, 2018.

SOLTANI, N. et al. Review on the physicochemical treatments of rice husk for production of advanced materials. **Chemical Engineering Journal**, v. 264, p. 899–935,

2015.

SONETAKA, N. et al. Characterization of adsorption uptake curves for both intraparticle diffusion and liquid film mass transfer controlling systems. **Journal of Hazardous Materials**, v. 165, n. 1–3, p. 232–239, 2009.

TAN, X. et al. Perchlorate uptake by wheat straw based adsorbent from aqueous solution and its subsequent biological regeneration. **Chemical Engineering Journal**, v. 211–212, p. 37–45, 2012.

TIAN, M. et al. Synthesis and characterization of thin film nanocomposite forward osmosis membranes supported by silica nanoparticle incorporated nanofibrous substrate. **Desalination**, v. 401, p. 142–150, 2017.

TRAN, H. N. et al. Mistakes and inconsistencies regarding adsorption of contaminants from aqueous solutions: A critical review. **Water Research**, 2017.

TSAI, W. T.; LEE, M. K.; CHANG, Y. M. Fast pyrolysis of rice husk: Product yields and compositions. **Bioresource Technology**, v. 98, n. 1, p. 22–28, 2007.

UEASIN, N.; LIAO, S.-Y.; WONGCHAI, A. The Technical Efficiency of Rice Husk Power Generation in Thailand: Comparing Data Envelopment Analysis and Stochastic Frontier Analysis. **Energy Procedia**, v. 75, p. 2757–2763, 2015.

UNUABONAH, E. I.; ADEBOWALE, K. O.; OLU-OWOLABI, B. I. Kinetic and thermodynamic studies of the adsorption of lead (II) ions onto phosphate-modified kaolinite clay. **Journal of Hazardous Materials**, v. 144, n. 1–2, p. 386–395, 2007.

USDA. **World Rice Production 2016/2017**. Disponível em: <https://www.worldriceproduction.com/>. Acesso em: 24 nov. 2017.

VANDER AUWERA, J. et al. Confinement-induced infrared absorption by H2 and N2 gases in a porous silica aerogel. **Journal of Quantitative Spectroscopy and Radiative Transfer**, v. 182, p. 193–198, 2016.

WANG, L.; YU, Q. Methane Adsorption on Porous Nano-silica in the Presence of Water: An Experimental and Ab Initio Study. **Journal of Colloid and Interface Science**, v. 467, 2015.

WANG, P. et al. Gelation of Ionic Liquid-Based Electrolytes with Silica Nanoparticles

for Quasi-Solid-State Dye-Sensitized Solar Cells. **Journal of american chemistry society**, p. 1166–1167, 2003.

WANG, Z. et al. **Textile dyeing wastewater treatmentIntech Open Science**. [s.l: s.n.]. Disponível em: <http://www.intechopen.com/source/pdfs/22395/intech-textile_dyeing_wastewater_treatment.pdf>.

WEBER, T.; CHAKRAVORTI, R. Pore and solid diffusion models for fixed-bed adsorbers. **American Institute of Chemical Engineers Journal**, v. 20, n. 2, 1974.

WU, Q. et al. Microchip-Based Macroporous Silica Sol - Gel Monolith for Efficient Isolation of DNA from Clinical Samples. **Analytical Chemistry**, v. 78, n. 16, p. 5704–5710, 2006.

XIA, J. et al. Rare-earth-doped silica microchip laser fabricated by sintering nanoporous glass. **Optics letters**, v. 30, n. 1, p. 47–9, 2005.

XIONG, L. et al. Burning Temperature Dependence of Rice Husk Ashes in Structure and Property. **Journal of Metals, Materilas and Minerals**, v. 19, n. 2, p. 95–99, 2009.

YAGUB, M. T. et al. Dye and its removal from aqueous solution by adsorption: A review. **Advances in Colloid and Interface Science**, v. 209, p. 172–184, 2014.

YALÇIN, N.; SEVINÇ, V. Studies on silica obtained from rice husk. **Ceramics International**, v. 27, n. 2, p. 219–224, 2001.

YAO, H. et al. Rheological Properties and Chemical Bonding of Asphalt Modified with Nanosilica. **Journal of Materials in Civil Engineering**, n. November, p. 1619–1630, 2013.

YOON, S. J. et al. Gasification and power generation characteristics of rice husk and rice husk pellet using a downdraft fixed-bed gasifier. **Renewable Energy**, v. 42, p. 163–167, 2012.

YUE, W.; ZHOU, W. Crystalline mesoporous metal oxide. **Progress in Natural Science**, v. 18, n. 11, p. 1329–1338, 2008.

YUREKLI, Y. et al. Filtration and removal performances of membrane adsorbers. **Journal of Hazardous Materials**, v. 332, p. 33–41, 2017.